Geochemical anomalies of critical elements (Be, Co, Hf, Sb, Sc, Ta, V, W, Y and REE) in soils of western Andalusia (Spain)

Juan Carlos Fernández-Caliani[a], Antonio Romero[b]; Isabel González[b]; Emilio Galán[b]

[a] Department of Earth Sciences, Faculty of Experimental Sciences, University of Huelva, Campus de El Carmen, 21071 Huelva, Spain

[b] Department of Crystallography, Mineralogy and Agricultural Chemistry, Faculty of Chemistry, University of Seville, Campus de Reina Mercedes, 41071 Seville, Spain

Abstract

A collection of 694 soil samples was taken from 367 sites (at a density of 1 site per 120 km^2) in the western of Andalusia (SW Spain) to establish regional geochemical background of emerging critical elements on the <2 mm soil fraction, and provide threshold values for anomaly detection to support mineral exploration in the survey area. The spatial distribution pattern of the soil geochemical anomalies is primarily influenced by the occurrence of magmatic alignments and metallogenic belts in the southern zones of the Iberian Massif. Soils over granitic parent materials are marked by W, Be, Ta and REE anomalies, whereas those derived from mafic igneous rocks contain anomalous concentrations of Sc, Co and V. Most of the threshold exceedances for Hf and Sb appear to be linked to soils on pelitic metasediments. The distribution of Sb and Co outliers is also related to sulfide ore occurrences in the bedrock and could be affected by anthropogenic influences. The Santa Olalla igneous complex, the granodioritic pluton of the Los Pedroches batholith and the magmatic alignment of Villaviciosa de Córdoba-La Coronada may represent exploration opportunities for high-tech elements, mainly for REE, although the identification of promising areas requires further investigation.

keywords: High-tech metals, geochemical baseline, threshold values, anomaly detection, soil exploration geochemistry.

1. Introduction

There are growing concerns about the long-term security of supplies of raw materials that are crucial to modern technology and society. Variously referred to as critical, strategic or high-tech metals and metalloids, these elements are currently produced in small quantities as by-products, they are increasingly used in a range of high-technology and clean energy applications, and have no effective substitutes (Graedel et al., 2015). The risks of supply shortage and their impacts on the global economy are higher compared with most of the other raw materials, due to the fact that a high share of the worldwide production is only concentrated in a few countries, with China being the leading supplier.

Criticality is a subjective and dynamic concept. Each country or groups of countries develop their own lists of critical elements and minerals based on their industrial and strategic interests (Hayes and McCullough, 2018). Criticality assessments are subject to change with time and hence that lists are subject to regular update and revision. In Septembre 2017, the European Commission (EU) issued an updated list of critical raw materials with a high supply-risk and a high economic importance for the European Union (European Commission, 2017), which is used to incentivise the production of strategic minerals and metals and facilitate the launching of new mining and recycling activities. Some elements listed by the EC include: Be, Bi, Co, Ga, Ge,

Hf, In, Mg, Nb, P, Sb, Sc, Ta, V, W, Y, platinum-group metals (PGM) and rare earth elements (REE). They are increasingly used in the manufacture of mobile phones and computers, LCD screens, electric cars, solar panels, rechargeable batteries, medical devices and many other high-tech applications and products. All these elements are located within the criticality zone (supply risk ≥ 1 and economic importance ≥ 2.8) of Figure 1.

Most of the critical elements are typically found in low concentrations in primary ore deposits of major metals but they are cycled during chemical weathering, pedogenesis and other surface processes, hence soil and regolith developed on mineralized bedrock areas can be enriched in such elements (Jowit et al., 2017, Négrel et al., 2019). Thus, for instance, clay deposits and clayey soils containing high concentrations of exchangeable REE that are thought to be adsorbed on clay minerals, dominantly kaolinite and halloysite, have become a critical mineral resource in China (Bao and Zhao, 2008). Therefore, the identification of significant geochemical anomalies in soils and weathering crusts is a key issue in mineral exploration of high-tech elements.

Andalusia is a region in the South of Spain with a long history of mineral exploration and mining, particularly for pyrite and iron oxides, and it is currently a major contributor to world supply of base metals, notably Cu, Pb and Zn. However, the potential for trace elements that are regarded as critical has not been assessed. Andalusia's geology is relatively well endowed with a wide variety of mineral deposit styles and thought to be prospective for a range of commodities (García-Cortés et al., 2011). Its potential for discovering new deposits of strategic metals and metalloids in

soil and regolith profiles remains high, but the occurrence, extent and grade of these non-conventional deposits are not well known or not published.

This paper was intended to improve the knowledge base of critical raw materials resources and their potential in western Andalusia, highlighting areas for future research in geochemical prospecting. The main objectives were: 1) to define the soil geochemical baseline of selected critical elements; 2) to provide threshold values for anomaly detection; and 3) to explain the source and factors influencing the distribution of the major soil geochemical anomalies.

2. Regional bedrock geology

The survey area encompasses about 45,400 km^2 of the western provinces of Andalusia, namely Huelva, Sevilla, Cádiz and Córdoba, covering a large part of southwestern Spain (Fig. 2). The most common soils across the study area are Cambisols, Leptosols and Regosols (WRB, 2014). The geology of the area can be delineated into three major zones representing distinct geotectonic environments: 1) the Iberian Massif, widely exposed across the north, consisting mainly of Palaeozoic sedimentary formations that were metamorphosed and deformed during the Variscan orogeny and intruded by granitoids; 2) the Betic Cordillera to the south where the geology is dominated by Mesozoic and Cenozoic sediments deformed by the Alpine tectonics; and 3) the Guadalquivir Basin, an elongated foreland basin developed during the Neogene and Quaternary between the Iberian Massif and the Betic Cordillera.

103 The basement terranes outcropping in the study area correspond to three
104 tectonostratigraphic zones of the Iberian Massif (Julivert et al., 1972): Central-Iberian
105 Zone, Ossa-Morena Zone and South-Portuguese Zone, which are the westernmost
106 exposures of the European Variscan Belt. On the other hand, the outcropping rocks of
107 the Betic Cordillera belong to the Subbetic Domain of the External Zone and the flysch
108 units of the Campo de Gibraltar Complex. A comprehensive review of the regional
109 geological setting can be found in Gibbons and Moreno (2002) and Vera (2004). Here
110 are summarized the main lithologic features and the metallogenic framework of the
111 bedrock areas.
112
113 The Central-Iberian Zone (CIZ) is characterized by the occurrence of a long
114 elongated magmatic body known as Los Pedroches batholith (e.g. Donaire et al., 1999),
115 consisting of a granodiorite pluton, a dyke swarm and a suite of monzogranite plutons
116 that intruded into low-grade metamorphic rocks of Late Precambrian to Carboniferous
117 ages. The host rocks belong to an Early Carboniferous sequence composed of
118 alternating slates and greywackes (facies Culm). To the north of the batholith, the
119 Precambrian basement is formed by a thick succession of schists and greywackes, while
120 to the south there is a series of black schists and metagreywackes with intercalations of
121 amphibolites and volcanic-sedimentary rocks. These are, in turn, unconformably
122 overlain by Cambrian carbonatic and siliciclastic sediments. The batholith encloses
123 many hydrothermal vein-type deposits that have been mined in ancient times for a
124 variety of valuable metals like Cu, Pb, Zn, Ag, Sn, W, Sb, Co and Bi (Locutura et al.,
125 1990).
126

The Pre-Ordovician rocks of the Ossa-Morena Zone (OMZ) are similar to those described for the south CIZ of the Los Pedroches batholith. The Ordovician-Silurian-Devonian sucessions consist mainly of slates, sandstones, black shales and quartzites, while the Upper Devonian-Carboniferous syn-orogenic sediments are dominated by turbidites with minor volcanic and conglomeratic intercalations. The complex geological evolution of the OMZ has produced a wide range of mineralization styles (Tornos et al. 2004), including volcanic-hosted massive sulfides (VHMS), sedimentary-exhalative deposits, skarns and replacements, orthomagmatic ore bodies, and a variety of metal-bearing hydrothermal veins.

The South-Portuguese Zone (SPZ) is the southernmost tectonic segment of the Iberian Massif. The most remarkable feature of the SPZ is the occurrence of several VHMS deposits of world-class importance forming the Iberian Pyrite Belt (IPB). The oldest rocks exposed within the IPB form a terrigenous sedimentary sequence composed of phyllites and quartzites with some limestone lenses at its top of Upper Devonian age, which is overlain by bimodal volcanic rocks within a sedimentary framework. This volcanic-sedimentary complex is covered by turbiditic sediments (flysch deposits) with an Early Carboniferous age, and it is the host for the VHMS deposits and numerous manganese occurrences. About 60 mines have operated during the last century mainly for pyrite, although most orebodies contain appreciable amounts of Cu, Pb and Zn, precious metals and a wide variety of trace elements, such as As, Bi, Cd, Co, Hg, Sn, and Se (e.g. Leistel et al., 1998; Tornos, 2006).

The External Zone of the Betic Cordillera corresponds to the Mesozoic and Tertiary sedimentary cover of the Iberian Massif. The Subbetic domain of the External

Zone forms a complex of thrust nappes comprising Triassic to Middle Miocene sedimentary successions with local volcanic and subvolcanic mafic rocks. In general, the Triassic terrains are composed of red detrital sediments and evaporites, the Jurassic is represented by marine carbonate deposits (dolostones and limestones), and the Cretaceous is characterized by a predominance marly limestones. The flysch units of the Campo de Gibraltar Complex (CGC) contain a series of tectonic units, mainly turbiditic, and olithostrosmal formations which range from Cretaceous to Early Miocene.

Finally, the Neogene infill of the Guadalquivir Basin comprises five offlapping depositional sequences that are progressively younger to the west (Sierro et al., 1996). The basin is filled with autochthonous sediments (calcarenites, bioclastic limestones, clays, silts and sands) that unconformably overlie the Iberian Massif, and allochthonous units consisting of gravity-flow deposits (olistostromes) linked to the southern active margin, as a result of the dismantling and erosion of the overthrusted nappes from the Betic Cordillera.

3. Soil sampling and methods

A total of 694 soil samples were collected from 367 sites unevenly distributed over the study area, with a sampling density of about one site per 120 km^2. In an attempt to reduce selection bias, the sample locations were chosen using a stratified random sampling strategy based on bedrock geology, as lithology of the parent materials is the main soil-forming factor controlling the soil geochemistry in the area (e.g. Galán et al., 2008). The sites were chosen to represent rural areas with no direct source of pollution other than atmospheric deposition and diffuse contamination from human activities.

177 Sampling was avoided in agricultural ecosystems to prevent contamination from
178 fertilizers.
179
180 Soil core samples were taken with an Edelman auger from a depth of 0-20 cm
181 (367 topsoil samples) at all sites, and from a depth of 20-40 cm (327 subsoil samples) in
182 those locations where the bedrock was encountered at greater depths below the ground
183 surface. In order to improve statistical confidence, the samples were bulked in the field
184 to make a composite sample of about 4 kg per depth interval, at each site, from five soil
185 cores collected in crossing directions and spaced approximately 1.5 m around the
186 central sampling position. The soil samples were dried at ambient air temperature,
187 gently disaggregated with a wooden roller, sieved to pass a 2-mm stainless steel screen
188 and then thoroughly mixed to ensure homogeneity. A subsample of each sieved soil was
189 ground using an agate mortar to recover the less than 63 μm grain-size powder for
190 chemical analysis.
191
192 The samples were analyzed for Be, Co, Hf, Sb, Sc, Ta, V, W, Y and some REE
193 (La, Ce, Nd, Sm, Eu, Tb, Yb and Lu) at Activation Laboratories Ltd. (Ontario, Canada),
194 which is accredited to the ISO/IEC 17025 Quality System. For all the elements, except
195 Be, V and Y, total concentrations were determined by instrumental neutron activation
196 analysis (INAA). A 30 g sample was irradiated at a thermal flux of 7 x 10^{12} neutrons
197 cm^{-2} s^{-1}. After a seven-day decay period, the samples were counted on a high resolution
198 Ge detector. The decay-corrected activities were compared to a calibration obtained by
199 using multiple certified international reference materials. From 10-30% of the samples
200 were rechecked by re-measurement and one standard was run for every 11 samples.
201 Yttrium, V and Be determinations were conducted by inductively coupled plasma-

optical emission spectrometry (ICP-OES), after a multi-acid digestion ($HClO_4$-HNO_3-HCl-HF) at 260º C. Quality control of the analytical procedure included the use of a method reagent blank, duplicates and certified reference materials to ensure accuracy and precision of results. The relative deviations of the standard analyses to the reference values were typically below 10%.

A statistical evaluation of the analytical data, including descriptive statistics, univariate and multivariate correlation analysis, and outlier detection, was applied in this study. In order to reduce bias in the statistical analysis, non-detectable values were replaced by half of the detection limit values. Since the element concentrations showed a wide range of variation, the median value was considered to be representative of the baseline. The upper limit of baseline variation was determined by using the median value plus double median absolute deviation (Me + 2MAD), which is much more robust against the effect of data outliers (Reimann et al., 2005; Reimann and De Caritat, 2017; Vural, 2019). The inter-element relationships were evaluated and quantified by principal component analysis (PCA). The approach used here for outlier detection is based on the upper inner fence or upper whisker in a Tukey boxplot (ISO, 2005). Thus, the upper inner fence (UIF) was calculated as follows:

$$UIF = Q3 + 1.5 \times IQR$$

where Q3 is the third quartile (75^{th} percentile) and IQR is the interquartile range (difference between 75^{th} and 25^{th} percentiles). The UIF is usually considered the threshold separating baseline values and mild anomalies (Reimann et al., 2005; Carranza, 2009). All values above the upper outer fence (UOF), which lie more than

three times the interquartile above the third quartile (UOF = Q3 + 3.0 x IQR), are referred to as far outliers, and they correspond to extreme anomalies.

4. Results and discussion

The concentrations of critical elements in soils of the survey area vary greatly spatially from one sampling site to another. A descriptive statistical summary of the results, showing the commonly used measures of central tendency (arithmetic mean, median and mode) and dispersion or variability (standard deviation and range), is given in Table 1. Average content of the critical elements in the upper continental crust and their median concentrations in soils of western Europe (data from the Forum of European Geological Surveys -FOREGS- database) have been also included in Table 1 for comparative purposes. The same statistical parameters of the measured concentrations are reported in Table 2, but categorized by geological domains, in order to show the influence of the underlying regional geology on soil geochemical baselines and threshold values for the critical elements under consideration. The upper limit of baseline concentration, defined by the Me + 2MAD, are also provided in Table 1 and Table 2.

Threshold values for mild and extreme anomalies corresponding to inner (UIF) and outer (UOF) fences, respectively, are given in Table 3, as well as the number of anomalous samples detected for each element in topsoil and subsoil. In the case of Be and W, the threshold values separating geochemically anomalous soil samples from baseline were the 95^{th} and 98^{th} percentiles, because their median values were below the lower detection limits. All of the anomalous concentrations were collated to produce

anomaly distribution maps of the selected critical elements (Fig. 3). These maps are useful in highlighting areas of potential interest for further exploration, where concentrations exceed the threshold values.

Several clusters are apparent on the projection of the scores on the first two factors extracted from the PCA, after Varimax rotation (Fig. 4). Together, Factor 1 and Factor 2 accounted for 62.2% (topsoil samples) and 66.9% (subsoil samples) of the variability among the elements, and they have allowed us to establish distinctive pedogeochemical associations in both sampling levels. Factor 1 is characterized by strong positive loadings (greater than 0.8) for REE and Y (REY). The concentrations of REY showed a high degree of positive correlation ($p < 0.05$) among themselves, suggesting similar geochemical behaviour in the soil system. On the other hand, Factor 2 revealed two clusters defined by opposite scores: Be-W-Ta-Hf and Co-Sc-V. These geochemical associations are interpreted as formed by critical elements associated to acid and basic igneous rocks, respectively, suggesting lithological discrimination between felsic and mafic sources.

4.1 Geochemical baseline variation, thresholds and anomalies

Rare Earth Elements and Ytrium (REY)

As expected, Ce was the most abundant element of the lanthanide group in the soils although its concentration, as well as those of the other REE, varied almost two orders of magnitude among sampling sites. The spatial distribution of REE is similar in the topsoil across the region, as previously noted by Locutura et al. (2012), although

277 there are important differences between light rare earth elements (LREE) and heavy rare
278 earth elements (HREE). Relatively high levels above the baseline concentrations of Ce
279 (107 mg kg^{-1}), La (52.8 mg kg^{-1}), Nd (42 mg kg^{-1}), Sm (8.6 mg kg^{-1}), Eu (1.8 mg kg^{-1}),
280 Yb (4.4 mg kg^{-1}), Lu (0.69 mg kg^{-1}) and Y (23 mg kg^{-1}) were found in Cambisols
281 developed over granitic rocks of the Los Pedroches batholith and in shallow lithic
282 Leptosols that are underlain by metasedimentary rocks of the CIZ, in the Iberian Massif.
283 These levels are well above the median of the REE concentrations in Spanish and
284 worldwide soils (Locutura, 2012; Reimann and De Caritat, 1998).
285
286 Cambisols of the Los Pedroches valley are relatively enriched in HREE (up to
287 11.3 mg kg^{-1} of Yb, 2.6 mg kg^{-1} of Tb and 1.6 mg kg^{-1} of Lu) relative to regional
288 geochemical baseline, suggesting that residual zircon plays a dominant role in
289 accumulating HREE in soil. However, the highest concentrations of LREE (up to 332
290 mg kg^{-1} of Ce, 169 mg kg^{-1} of La, 114 mg kg^{-1} of Nd and 332 mg kg^{-1} of Sm) were
291 measured in soils developed on tonalitic rocks from an intrusive stock emplaced in the
292 OMZ, the so-called Santa Olalla Igneous Complex (Romeo et al., 2006) in Huelva
293 province. The LREE-enriched granitoids are often abundant in apatite, monazite, titanite
294 and allanite formed by magma differentiation (Li et al., 2017). Interestingly, the largest
295 abundances of Eu (13.6 mg kg^{-1}) and Y (103 mg kg^{-1}) occurred in soils on carbonate
296 rocks of the external zone of the Betic Cordillera. When categorized by geological
297 setting, the baseline concentrations of REE in the CIZ were markedly greater than in
298 any of the other zones.
299
300 *Beryllium (Be), tungsten (W), tantalum (Ta) and hafnium (Hf)*
301

Total concentrations of Be, W and Ta were below their respective lower detection levels in the vast majority of soil samples because they are relatively scarce trace elements. The content of Be hardly amounted to more than 2 mg kg^{-1}. The largest concentrations of this lightweight metal (up to 10 mg kg^{-1}) were found in Cambisols and Arenosols derived from coarse-grained crystalline rocks of granodioritic composition belonging to the Los Pedroches batholith. In this area, the upper limit of geochemical baseline variation was 6.7 mg kg^{-1}. Some of the most anomalous concentrations of Be may be due to the occurrence of beryl mineralization in granitic pegmatites. An extreme outlier for Be was also detected in Leptosol developed on slates and quartzites of the SPZ, in both levels of sampling, indicating a probable relation with local quartz-vein type Sn-W-As mineralization (Sáez et al., 1989).

The contents of W measured in soil were generally low to very low, with 85% of the topsoil samples having a concentration below the detection limit (<1 mg kg^{-1}). The soils over the Los Pedroches granodiorite are enriched in W relative to other areas of western Andalusia, reaching levels as high as 113 mg kg^{-1}. The mineralogical sources of the W anomalies are linked to intra- and perigranitic wolframite-bearing hydrothermal quartz veins (Tornos, 2004), associated with late Variscan peraluminous magmatism. An extreme outlier was also recognized on soils developed over mineralized igneous bodies forming the magmatic alignment of Villaviciosa de Córdoba-La Coronada (Pascual and Perez-Lorente, 1987), in Córdoba province. Interestingly, an elevated concentration of W (108 mg kg^{-1}) was detected locally in Leptosols of the Iberian Pyrite Belt, around stratabound scheelite occurrences (Sáez et al., 1988).

Likewise, the concentrations of Ta measured in topsoil were very low, with 65%

of the samples having a concentration of less than 1 mg kg^{-1}, and 57% of the samples being under the lower detection limit of 0.5 mg kg^{-1}. Relatively high levels of Ta (3.9 mg kg^{-1}) were observed in soils developed on granite bedrock, where this critical metal may occur in Ta-bearing granitic pegmatites in association with Nb, Li, Be, W and REY (Ercit, 2005).

The content of Hf in topsoil ranged largely from less than 1 up to 43 mg kg^{-1}, with the upper limit of baseline variation being 10 mg kg^{-1} in both topsoil and subsoil. Although, soils on Precambrian and Lower Paleozoic metasedimentary rocks of the CIZ had the largest mean concentrations of Hf, the maximum value was measured in sandy soils of the Lower Guadalquivir Basin. The upper outer fence for Hf (28 mg kg^{-1}) was surpassed at three sampling sites. In all cases, the extreme values may have a geogenic origin related to coarse-textured unconsolidated sediments and weakly developed mineral soils (Regosols). Because of Hf and Zr have nearly identical charge and ionic radii, it can be assumed that Hf is mainly locked up in detritic zircon, a common heavy mineral inherited from granitic parent rock in soil.

Cobalt (Co), scandium (Sc) and vanadium (V)

The median Co content in topsoil was 13 mg kg^{-1}, with a range from 2 to 59 mg kg^{-1}; the total Sc concentration ranged between 0.2 and 44.9 mg kg^{-1}, with a median value of 10.8 mg kg^{-1}, whereas the total V concentration showed a greater variability, within two orders of magnitude (from less than 2 mg kg^{-1} up to 383 mg kg^{-1}), with a median of 78 mg kg^{-1}. The median concentrations of Co, Sc and V are above the median of the European and Spanish soils (Salminen, 2005; Locutura, 2012). The spatial

distribution patterns of these metals are rather similar, as they appear strongly correlated with linear correlation coefficients as high as 0.80-0.91 ($p < 0.05$).

Relatively high levels of Co (up to 59 mg kg^{-1}), Sc (44.9 mg kg^{-1}) and V (383 mg kg^{-1}) were measured in the OMZ, whereas the lowest levels were found in soils of the Guadalquivir Basin. The greatest abundances of Co, Sc and V in soils seem to be related to the occurrence of underlying mafic igneous rocks, mainly basalts, gabros and metabasites derived from basaltic lavas, particularly in the SPZ and OMZ zones. Hence, their spatial distribution appears to be controlled by the parent rock lithology.

The extreme anomalies of Co, V and Sc in the OMZ occurred at the top of the soils developed on the Acebuches amphibolites, in the Aracena metamorphic belt (Castro et al., 1996). Relatively high concentrations of Co were also found in Leptosols of the SPZ linked to acid volcanic and volcano-sedimentary parent rocks, in which the VHMS deposits of the Iberian Pyrite Belt are hosted. A range of critical elements, including Co may be contained in the base metal mineralization.

Antimony (Sb)

The total Sb content in topsoil samples varied largely from less than 0.1 mg kg^{-1} to 318 mg kg^{-1}, with a median value markedly low (1 mg kg^{-1}). Baseline concentrations of Sb ranged up to 6.6 mg kg^{-1} in the SPZ and 4.5 mg kg^{-1} in the OMZ, exceeding significantly those of the European soils. There is no apparent association with a specific lithology in the distribution of Sb and it did not show a linear correlation in its spatial distribution with any of the other analyzed elements.

377

378 The contents of Sb in the samples of the SPZ are widely spread from the mean
379 (16.2 ± 51.5 mg kg^{-1}) due to its inhomogeneous distribution in topsoil. The highest Sb
380 concentrations (above 100 mg kg^{-1}) were measured in Leptosols of the Iberian Pyrite
381 Belt, due to naturally occurring Sb-bearing sulfides and sulfosalts in mineralized
382 bedrock. They can be attributed not only to geogenic origin but probably also to diffuse
383 contamination associated with past mining activities. In fact, some mines were
384 historically worked for Sb (Leistel et al., 1998), which may occurs as locally dispersed
385 in soil. In the OMZ zone, the greatest abundances of Sb were found in topsoil formed
386 from weathering of carbonate rocks rather than igneous rocks or metasediments. There
387 is a good spatial correspondence between high concentrations of Sb in topsoil and
388 location of the Pb-Zn-Ag metallogenic belts of the OMZ zone (Tornos et al., 2004,
389 Fernández-Caliani et al., 2019).

390

391 Outlier and extreme values for Sb were also detected in peri-urban contaminated
392 soils of Huelva, one of the first industrial cities in Spain (Fernández-Caliani, 2012),
393 where the most obvious cause of the anomalous concentrations is anthropogenic. In
394 addition, an extreme Sb anomaly was identified in the Campo de Gibraltar Complex
395 that is difficult to explain without further investigation.

396

397 4.2 Vertical distribution of critical elements within the soil profile

398

399 Variability of elements concentrations within the soil profile was low.
400 Differences between the median values of the two soil sampling levels were relatively
401 small for most critical elements, as indicated by a ratio topsoil/subsoil from slightly

above the unity to 1.15, thus providing a lithological cause for most anomalies as the concerned elements have limited mobility in soil. Exceptionally, Sb (1.25) and Co (1.18) were found in greatest concentrations in topsoil relative to subsoil, most likely due to anthropogenic contributions, although such surface enrichments require a high-density geochemical survey to trace their source. In fact, since some Co-bearing and Sb-bearing ore deposits have been mined historically in the region, it is difficult to evaluate whether anomalies are natural in origin or mining has exacerbated the original mild anomalies.

The concentrations of critical elements in topsoil and subsoil were positively and strongly correlated, most notably for Sb, Sc, V, Hf and Co. The Pearson´s correlation coefficients given in Figure 5 allowed us to evaluate the linear relationships between topsoil and subsoil samples, and then the spatial variability in concentrations of critical elements within the soil profile. Despite most REE are usually immobilized in weathering resistant primary minerals (Galán et al., 2007), such as zircon, monazite, xenotime, some topsoil samples appear to be REE-depleted. This is particularly true for Ce, because Ce(III) can be easily oxidized to Ce(IV) under the oxidizing conditions prevailing in the surface soil, and subsequently retained in subsoil onto clay minerals.

4.3 Some factors controlling the spatial distribution of anomalies

In an attempt to visualize the relationships between the abundance and spatial distribution of the measured critical elements and the underlying geology, Figure 6 depicts graphically the percentage of anomalous concentrations of critical elements according to the geological setting of the bedrock, lithology of the underlying parent

material and soil type. The observed distribution pattern of the mild and extreme anomalies certainly reflects the influence of the local geology on soil geochemistry, and especially the parent rock lithology and the occurrence of ore deposits hosting critical elements in the survey area.

Based on the available data, it is apparent that the areas of greatest interest for strategic metals in western Andalusia are found within the crystalline terranes of the Iberian Massif (Fig. 6a). The CIZ is the main prospective zone for Be and W, the OMZ contains promising areas for Co, Sc, V, Hf, Ta, and REE exploration, and the geological setting of the SPZ appears favorable for prospecting for Sb and, to a lesser extent, Co, V and Sc. Most of the anomalies of Be, W, Ta and REE are within the weathering crusts of granites and soils developed on margins of granitic intrusive bodies, whereas the most pronounced anomalies of Co, Sc and V were observed in soils derived from basic and ultrabasic rock throughout the terranes of the Iberian Massif. The outlier values of Hf and Sb were mostly found in soils on slates and schists, although a number of threshold exceedances for Hf was also related to sandy soils of the Gudalquivir Basin (Fig. 6b). Finally, the vast majority of geochemical soil anomalies were recorded in Cambisols and Leptosols with little or no profile differentiation (Fig. 6c).

5. Conclusions

The soil sampling strategy used in this exploratory study has allowed us to determine the geochemical baseline variation of selected critical elements in soil for distinctive geological environments, to provide threshold values for anomaly detection,

and to explain the source and factors influencing the distribution of the major soil geochemical anomalies.

Lithology of the underlying bedrock is inferred as the major source of geochemical anomalies, although abundance and spatial distribution of critical elements not only depends on the parent rock lithology, but also it is connected with local ore deposits and occurrences of a vast range of mineralization styles. Soils over peralkaline felsic igneous intrusions, distributed along tectono-magmatic alignments of the CIZ and ZOM, are clearly marked by W, Be, Ta and REE anomalies, whereas the anomalous concentrations of Sc, Co and V are closely associated with soils developed on mafic igneous rocks of the ZOM and SPZ. The Hf and Sb anomalies seem to be related to soils derived from pelitic metasediments. The distribution of high values of Sb and Co is also related to well-known massive sulfide ore occurrences, notably in the Iberian Pyrite Belt of the SPZ and in the metallogenic belts of the ZOM. Some spurious outliers and extreme values of Sb and Co may have been affected by anthropogenic inputs.

Prospective areas for REE resources are locally identified in the Santa Olalla Igneous Complex, where there is potential for forming REE deposits including ion-adsorbed type REE mineralization, residual primary and/or secondary REE-bearing minerals in well-developed weathering profiles of tonalite rocks. The granodioritic pluton of the Los Pedroches batholith and the plutonic-volcanic complex of Villaviciosa de Córdoba-La Coronada may also represent interesting prospective targets for high-tech metals, and should be investigated at a more detailed scale.

Acknowledgments

The findings presented in this paper were obtained in the framework of the Project "A Survey of Trace Element Concentrations in Soils of Andalusia", a research program led by Prof. Emilio Galán and financially supported by the Andalusia Government (Spain).

References

Bao, Z., Zhao, Z. 2008. Geochemistry of mineralization with exchangeable REY in the weathering crusts of granitic rocks in South China. Ore Geol. Rev. 33, 519-535.

Carranza, E.J.M., 2009. Geochemical Anomaly and Mineral Prospectivity Mapping in GIS. Handbook Exploration and Environmental Geochemistry, Vol. 11, Elsevier.

Castro, A., Fernández, C., De la Rosa, J.D., Moreno-Ventas, I., Rogers, G., 1996. Significance of MORB-derived amphibolites from the Aracena Metamorphic Belt. J. Petrol., 37, 235-260.

Donaire, T., Pascual, E., Pin, C., Duthou, J.L., 1999. Two-stage granitoid-forming event from an isotopically homogeneous crustal source: The Los Pedroches batholith, Iberian Massif, Spain. Geol. Soc. Am. Bull. 111, 1897-1906.

Ercit, T.S., 2005. REE-enriched granitic pegmatites. In: Linnen, R.L., Samson, I.M. (Eds), Rare-Element Geochemistry and Mineral Deposits. Geol. Ass. Canada, pp. 175-199.

European Commission, 2017. Study on the Review of the List of Critical Raw Materials: Criticality Assessments. Final Report, http://doi.org/10.2873/876644

Fernández-Caliani, J.C., 2012. Risk-based assessment of multimetallic soil pollution in the industrialized peri-urban area of Huelva, Spain. Environ. Geochem. Health, 34, 123-139.

Fernández-Caliani, J.C., Giráldez, M.I., Rivera, M.B., 2019. Source and geochemical partitioning of silver in a naturally-enriched soil. Appl. Geochem. 103, 85-96.

Galán, E., Fernández-Caliani, J.C., Miras, A., Aparicio, P., Márquez, M.G., 2007. Residence and fractionation of rare earth elements during kaolinization of alkaline peraluminous granites in NW Spain. Clay Min. 42, 341-352.

Galán, E., Fernández-Caliani, J.C., González, I., Aparicio, P., Romero, A., 2008. Influence of geological setting on geochemical baselines of trace elements in soils. Application to soils of South-West Spain. J. Geochem. Expl. 98, 89-106.

García-Cortés, A. (Ed.), 2011. Cartografía de Recursos Minerales de Andalucía. Instituto Geológico Minero de España - Consejería de Economía, Innovación y Ciencia de la Junta de Andalucía.

Gibbons, W., Moreno, T., (Eds.), 2002. The Geology of Spain. The Geological Society, London.

526

527 Graedel, T.E., Harper, E.M., Nassar, N.T. Nuss, P., Reca, B.K., 2015. Criticality of
528 metals and metalloids. PNAS, 112, 4257-4262.

529

530 Hayes, S.M., McCullough, E.A., 2018. Critical minerals: A review of elemental trends
531 in comprehensive criticality studies. Resour. Policy, 59, 192-199.

532

533 ISO (International Organization for Standardization), 2005. Soil Quality - Guidance on
534 the Determination of Background Values. International Standard ISO 19258: 2005(E)
535 24 pp.

536

537 Jowit, S.M., Wong, V.N.L., Wilson, S.A., Gore, O. 2017. Critical metals in the critical
538 zone: controls, resources and future prospectivity of regolith-hosted rare earth elements.
539 Austral. J. Earth Sci., 64, 1045-1054.

540

541 Julivert, M., Fontboté, J.M., Ribeiro, A., Conde, L., 1972. Mapa Tectónico de la
542 Península Ibérica y Baleares a escala 1:1.000.000. Memoria explicativa. IGME, Madrid.

543

544 Leistel, J.M., Marcoux, E., Thiéblemont, D., Quesada, C., Sánchez, A., Ruiz de
545 Almodóvar, G., Pascual, E., Sáez, R., 1998. The volcanic-hosted massive sulphide
546 deposits of the Iberian Pyrite Belt. Miner. Deposita 33, 2-30.

547

548 Li, Y.H.M., Zhao, W.W., Zhou, M.F., 2017. Nature of parent rocks, mineralization
549 styles and ore genesis of regolith-hosted REE deposits in South China: An integrated
550 genetic model. J. Asian Earth Sci. 148, 65-95.

Locutura, J., Bel-Lan, A., García-Cortés, A., Martínez, S., 2012. Atlas Geoquímico de España. Instituto Geológico y Minero de España, Madrid.

Locutura, J., Tornos, F., Florido, P., Baeza, L., 1990. Ossa-Morena Zone: Metallogeny. In: Martinez, E., Dallmeyer, R.D. (Eds), Pre-Mesozoic Geology of Iberia. Springer Verlag, pp. 321-332.

Négrel, P., Ladenberger, A., Reimann, C., Birke, M., Demetriades, A., Sadeghi, M., 2019. GEMAS: Geochemical background and mineral potential of emerging tech-critical elements in Europe revealed from low-sampling density geochemical mapping. Appl. Geochim. 111, 104425. doi.org/10.1016/j.apgeochem.2019.104425

Pascual, E., Pérez-Lorente, F., 1987. La alineación o eje magmático Villaviciosa de Córdoba-La Coronada. In: Bea, F., Carnicero, A., Gonzalo, J.C., López-Plaza, M., Rodríguez-Alonso, M.D. (Eds), Geología de los Granitoides y Rocas Asociadas del Macizo Hespérico. Rueda, Madrid, pp. 365-376.

Reimann, C., De Caritat, P., 1998. Chemical Elements in the Environment. Springer-Verlag, Berlin.

Reimann, C., De Caritat, P., 2017. Establishing geochemical background variation and threshold values for 59 elements in Australian surface soil. Sci. Total Environ. 578, 633-648.

576 Reimann, C., Filzmoser, P., Garret, R.G., 2005. Background and threshold: critical
577 comparison of methods of determination. Sci. Total Environ. 346, 1-16.
578
579 Romeo, I., Capote, R., Tejero, R., Lunar R., Quesada, C., 2006. Magma emplacement in
580 transpression: The Santa Olalla Igneous Complex (Ossa-Morena Zone, SW Iberia). J.
581 Struct. Geol. 28, 1821-1834.
582
583 Rudnick, R.L., Gao, S., 2004. Composition of the Continental Crust. In: Holland, H.D.,
584 Turekian, K.K. (Eds), Treatise on Geochemistry, Elsevier, Amsterdam, Vol. 3, pp. 1-64.
585
586 Sáez, R., Almodóvar, G.R., Pascual, E., 1988. Mineralizaciones estratoligadas de
587 scheelita en la Faja Pirítica del Suroeste Ibérico. Bol. Soc. Esp. Min. 11, 135-141.
588
589 Sáez, R., Requena, A., Fernández-Caliani, J.C., Almodóvar, G.R., 1989, Control
590 estructural de las mineralizaciones de Sn-W-As del Bajo Corumbel, La Palma del
591 Condado, Huelva. Stvdia Geol. Salmant. Vol. Esp. 4, 189-203.
592
593 Salminen, R., (Ed.), 2005. Geochemical Atlas of Europe. Part 1: Background
594 Information, Methodology and Maps. Geological Survey of Finland.
595 http://www.gtk.fi/publ/foregsatlas
596
597 Sierro, F.J., González-Delgado, J.A., Dabrio, C., Flores, J.A. y Civis, J., 1996. Late
598 Neogene depositional sequences in the forelandbasin of Guadalquivir (SW Spain). In:
599 Friend, P.F., Dabrio, C.J., (Eds), Tertiary basins of Spain, the stratigraphic record of
600 crustal kinematics. Cambridge Univ. Press, pp. 339-345.

Tornos, F., 2006. Environment of formation and styles of volcanogenic massive sulfides: The Iberian Pyrite Belt. Ore Geol. Rev. 28, 259-307.

Tornos, F., Inverno, C.M.C., Casquet, C., Mateus, A., Ortiz, G., Oliveira, V., 2004. The metallogenic evolution of the Ossa-Morena Zone. J. Iberian Geol. 30, 143-181.

Vera, J.A. (Ed.), 2004. Geología de España. Sociedad Geológica de España-Instituto Geológico Minero de España, Madrid.

Vural, A. (2019). Evaluation of soil geochemistry data of Canca Area (Gümüşhane, Turkey) by means of Inverse Distance Weighting (IDW) and Kriging methods-preliminary findings. Bull. Min. Res. Exp. 158, 195-216.

WRB, 2014. World Reference Base for Soil Resources 2014. International soil classification system for naming soils and creating legends for soil maps. World Soil Resources Reports 106. FAO, Rome. http://www.fao.org/3/i3794en/I3794en.pdf.

620 **FIGURE AND TABLE CAPTIONS**

621

622 Figure 1. Economic importance (EI) and supply risk (SR) of critical raw materials for
623 the European Union (modified after European Commission, 2017). Critical raw
624 materials are located within the criticality zone (SR ≥ 1 and EI ≥ 2.8) of the graph. The
625 critical elements analyzed in this study are highlighted by red dots. Abbreviations:
626 LREE (Light Rare Earth Elements). HREE (Heavy Rare Earth Elements). PGM
627 (Platinum Group Metals).

628

629 Figure 2. Simplified geological map of the study area and location of the sampling sites.

630

631 Figure 3. Geochemical anomaly maps of critical elements in topsoil samples.

632

633 Figure 4. Plot of the Principal Component Analysis showing variable loadings of the
634 first two factors for critical elements in topsoil samples.

635

636 Figure 5. Bivariate plots showing the relationship between concentrations of critical
637 elements in topsoil and subsoil. Outliers according to Tukey's inner fence criteria are
638 indicated by open circles, and the values beyond the upper outer fence (extreme
639 anomalies) are marked with asterisks.

640

641 Figure 6. Percent distribution of detected outliers by considering: a) geological setting;
642 b) parent rock lithology; and c) and soil type (WRB-FAO classification system).

643

644

645

646 Table 1. Descriptive statistical parameters for concentrations of critical elements in soil
647 samples categorized by topsoil and subsoil.

648

649 Table 2. Descriptive statistical parameters of the measured concentrations of critical
650 elements grouped by geological domains.

651

652 Table 3. Threshold values for mild (UIF) and extreme (UOF) anomalies and number of
653 threshold exceedances.

654

655

Table 1
Click here to download Table: Table 1.docx

Table 1

Element (mg kg^{-1})	**Be**	**Co**	**Hf**	**Sb**	**Sc**	**Ta**	**V**	**W**	**La**	**Ce**	**Nd**	**Sm**	**Eu**	**Tb**	**Yb**	**Lu**	**Y**
Lower limit of detection	2	1	1	0.1	0.1	0.5	2	1	0.5	3	5	0.1	0.2	0.5	0.2	0.05	1
Topsoil (0-20 cm)																	
Number of samples	304	367	304	304	304	304	304	304	304	304	304	304	304	304	304	304	304
Mean	<2	14.4	7.9	4.2	12.2	0.8	88.4	1.8	35.7	71.4	28.7	5.9	1.3	0.6	3.1	0.47	17
Median	<2	13	6	1.0	10.8	<0.5	78	<1	31.6	64	26	5.4	1.2	<0.5	2.7	0.43	14
Std. Deviation	<2	9.1	5.7	21.6	7.7	0.7	54.8	9.1	19.4	38.2	14.8	2.8	0.6	0.4	1.6	0.24	10.7
Minimum	<2	2	<1	<0.1	0.2	<0.5	<2	<1	2.1	4	<5	0.3	<0.2	<0.5	<0.2	<0.05	<1
Maximum	10	59	43	318	44.9	3.9	383	113	169	332	114	16.9	5.9	2.6	11.3	1.6	103
Mode	<2	8	5	0.7	8.2	<0.5	76	<1	32.9	107	26	5.1	0.9	<0.5	2.7	0.31	13
Upper background limit*	3	23	10	2.0	19	<0.5	137	<1	52.8	107	42	8.6	1.8	<0.5	4.4	0.69	23
Subsoil (20-40 cm)																	
Number of samples	202	327	202	202	202	202	202	202	202	202	202	202	202	202	202	202	202
Mean	<2	13.5	7.6	3.7	11.1	0.7	82.7	1.3	34.5	67.6	27.1	5.6	1.1	0.5	2.9	0.45	16.1
Median	<2	11	6	0.8	9.4	<0.5	72	<1	30.3	59	25	5.1	1.1	<0.5	2.4	0.38	13
Std. Deviation	<2	9.2	5.6	18.7	6.8	0.8	49.1	2.6	19	35.9	14.7	3.1	0.5	0.4	1.8	0.27	11.0
Minimum	<2	1	<1	<0.1	0.4	<0.5	4	<1	1.1	4	<5	0.2	<0.2	<0.5	<0.2	<0.05	<1
Maximum	8	52	34	200	35	4.9	225	19	98.6	194	92	24.8	2.9	3.6	13.9	2.06	87
Mode	<2	9	5	0.7	5.8	<0.5	50	<1	35.6	56	19	4.7	1.1	<0.5	2.3	0.38	6
Upper background limit *	2.3	21	10	1.4	16.6	<0.5	135	<1	48.9	97	39	8.1	1.7	<0.5	4.0	0.62	23
Reference values																	
Upper continental crust[1]	1.9	25	3.7	0.4	14	0.7	138	1.9	31	63	27	4.7	1.0	0.7	1.96	0.31	21
Topsoil[2]	<2	7.78	5.55	0.60	8.21	0.76	60.4	<5	23.5	48.2	20.8	3.96	0.77	0.60	1.99	0.30	21
Subsoil[2]	<2	8.97	5.30	0.47	9.19	0.75	62.8	<5	25.6	53.7	22.4	4.38	0.84	0.64	2.13	0.31	23

* Median + 2 Median Absolute Deviation
[1] Rudnick and Gao (2004). [2] Median concentrations in the FOREGS samples (Salminen, 2005).

Table 2

Click here to download Table: Table 2.docx

Element (mg kg^{-1})	**Be**	**Co**	**Hf**	**Sb**	**Sc**	**Ta**	**V**	**W**	**La**	**Ce**	**Nd**	**Sm**	**Eu**	**Tb**	**Yb**	**Lu**	**Y**
CENTRAL-IBERIAN ZONE																	
Number of samples	22	26	22	22	22	22	22	22	22	22	22	22	22	22	22	22	22
Mean	4	17.2	12.5	2.1	12.0	1.4	78.3	9.9	53.1	106.3	42.2	8.3	1.7	0.8	4.0	0.62	19.9
Median	3	15	11	1.6	9.7	1.5	60	5	56.7	115	44	9.5	1.9	1.0	4.4	0.74	17
Std. Deviation	2.1	11.1	8.1	1.6	8.7	1.0	60.7	24	19.4	37.9	16.1	3.3	0.7	0.6	2.0	0.29	9.8
Minimum	<2	5	4	0.5	3.2	<0.5	12	<1	14.7	34	14	3.4	0.7	<0.5	0.9	0.15	5
Maximum	10	49	36	6.1	43.2	3.2	247	113	82	160	69	14.2	2.8	1.6	8.7	1.20	37
Upper background limit	6.7	26	21	2.8	16.5	1.5	142	14	106.9	218	80	17.7	3.3	2.5	8.0	1.36	34
OSSA-MORENA ZONE																	
Number of samples	59	67	59	59	59	59	59	59	59	59	59	59	59	59	59	59	59
Mean	2.1	21.3	9.6	3.9	16.9	1.0	118	1.1	45.0	92.8	36.8	7.8	1.7	0.8	4.1	0.63	23.1
Median	2	19	8	2.2	15.1	<0.5	104	<1	44	88	36.5	7.6	1.5	0.9	3.8	0.58	21
Std. Deviation	1.0	11.0	6.5	5.1	8.6	0.9	65.5	1.9	25.3	51.9	18.1	3.0	0.9	0.5	1.7	0.27	9.5
Minimum	<2	2	1	<0.1	0.2	<0.5	2	<1	2.1	4	<5	0.3	<0.2	<0.5	0.1	<0.05	<1
Maximum	5.4	59	30	28.4	44.9	3.9	383	9	169	332	114	16.9	5.9	2.6	11.3	1.60	53
Upper background limit	3.7	31	14	4.5	24.3	<0.5	170	<1	78.3	149	63	12.3	2.4	2.1	6.3	0.94	34
SOUTH-PORTUGUESE ZONE																	
Number of samples	50	53	50	50	50	50	50	50	50	50	50	50	50	50	50	50	50
Mean	2	19.5	7.3	16.2	19.2	0.7	125	3.3	39.6	82.0	31.9	6.8	1.36	0.7	3.9	0.59	17.3
Median	2	18	7	2.9	17.8	<0.5	122	<1	42.1	85.5	31.5	6.9	1.4	0.7	3.8	0.55	13.6
Std. Deviation	0.9	9.6	2.8	51.5	7.5	0.7	56.9	15.2	16.6	31.2	12.9	2.2	0.4	0.4	1.2	0.19	11.3
Minimum	<2	2	3	<0.1	7.3	<0.5	16	<1	9.9	21	<5	1.8	0.4	<0.5	2	0.29	5
Maximum	5.7	43	15	318	40.4	3.1	289	108	83.4	154	73	15	2.6	1.8	7.2	1.10	61
Upper background limit	3.7	30	9	6.6	31.8	<0.5	218	<1	69.2	140	53	10.2	1.9	1.5	6.0	0.81	26

Element (mg kg^{-1})	**Be**	**Co**	**Hf**	**Sb**	**Sc**	**Ta**	**V**	**W**	**La**	**Ce**	**Nd**	**Sm**	**Eu**	**Tb**	**Yb**	**Lu**	**Y**
GUADALQUIVIR BASIN																	
Number of samples	102	139	102	102	102	102	102	102	102	102	102	102	102	102	102	102	102
Mean	<2	9.8	7.3	1.4	7.7	0.6	61.3	0.6	27.6	55.1	22.6	4.5	0.9	<0.5	2.3	0.36	13
Median	<2	10	5	0.8	7.9	<0.5	60	<1	27.6	52	22	4.4	1.0	<0.5	2.1	0.33	13
Std. Deviation	0.5	5.1	6.1	2.9	3.7	0.5	29	0.5	11.8	25.5	9.8	2.0	0.4	0.3	1.1	0.18	6.4
Minimum	<2	2	1	0.2	0.9	<0.5	10	<1	5.2	9	<5	0.8	<0.2	<0.5	0.4	0.07	2
Maximum	3.9	30	43	28.7	16.8	2.8	155	4	79.9	150	61	13.6	2.2	1.7	6.5	1.10	39
Upper background limit	2.2	18	9	1.6	15.1	<0.5	110	<1	41.8	85	34	6.9	1.6	<0.5	3.5	0.58	20
EXTERNAL BETIC ZONE																	
Number of samples	40	50	40	40	40	40	40	40	40	40	40	40	40	40	40	40	40
Mean	1.2	13.1	4.6	0.9	9.4	0.4	67	0.7	31	53	24.5	4.9	1.0	0.5	2.4	0.38	19
Median	<2	12	4	0.8	8.6	<0.5	65	<1	27.4	50	23	4.4	0.9	<0.5	2.1	0.34	14
Std. Deviation	0.6	7.2	2.7	0.5	5.3	0.4	35.4	0.5	21.6	25	14.4	2.5	0.6	0.4	1.3	0.20	16.6
Minimum	<2	4	1	0.3	3.1	<0.5	24	<1	13.6	23	10	2.1	0.4	<0.5	0.9	0.14	6
Maximum	3	44	12	2.8	25.3	1.6	191	3	133	156	95	14.9	3.6	1.8	8.1	1.20	103
Upper background limit	2	21	10	1.5	15.6	<0.5	121	<1	43.9	86	35	7.3	1.6	<0.5	3.6	0.59	23
CAMPO DE GIBRALTAR COMPLEX																	
Number of samples	32	32	32	32	32	32	32	32	32	32	32	32	32	32	32	32	32
Mean	<2	14.4	8.2	0.9	10.4	1.0	93.3	0.7	32.7	67.3	24.5	4.9	1.1	<0.5	2.5	0.37	14
Median	<2	13	8	0.7	10.3	1.0	88	<1	31.9	65	23	4.4	0.9	<0.5	2.5	0.36	14
Std. Deviation	0.6	10.3	3.3	1.4	4.3	0.6	50.3	0.8	9.6	23.6	8.8	1.7	0.4	0.3	0.6	0.09	7.7
Minimum	<2	3	3	0.3	4.2	<0.5	31	<1	17.1	37	11	2.0	0.4	<0.5	1.3	0.22	5
Maximum	3	40	16	8.5	18.2	2.4	219	5	54.3	118	43	8.6	1.8	1.1	3.5	0.51	48
Upper background limit	2.6	29	14	1.5	16.9	1.0	137	<1	43.1	96	37	6.8	1.5	<0.5	3.3	0.52	21

Table 3

Click here to download Table: Table 3.docx

Element (mg kg^{-1})	95th Percentile	98th Percentile	Outliers (Q3+1.5IQR)	Number of mild anomalies	Far outliers (Q3+3IQR)	Number of extreme anomalies
TOPSOIL						
Be	4	5	-	12	-	6
Co	32	41	33	14	48	4
Hf	19	26	19	12	28	3
Sb	8.4	24.2	4.7	20	7.1	18
Sc	28.8	34.6	27.9	15	40.4	2
Ta	2.1	2.8	2.6	9	4.1	0
V	193	247	202	11	293	1
W	5.0	8.9	-	12	-	7
La	67.7	80.4	78	6	111	2
Ce	139	154	159	4	227	1
Nd	56	63	64	4	91	2
Sm	11.2	13.5	12.1	9	16.9	0
Eu	2.3	2.9	2.4	12	3.3	3
Tb	1.40	1.69	1.69	6	2.55	1
Yb	5.8	7.2	6.8	8	9.6	1
Lu	0.91	1.17	1.02	9	1.44	1
Y	37	44	34	17	47	4
SUBSOIL						
Be	4.2	6.5	-	6	-	5
Co	32	40	32	16	47	4
Hf	22	24	19	10	28	2
Sb	6.3	16.3	2.9	13	4.2	15
Sc	26.1	31.9	27.3	9	49.9	0
Ta	2.0	3.3	2.4	5	3.7	2
V	175	196	204	3	299	0
W	6.0	9.0	-	7	-	4
La	71.7	90.6	71.1	11	100.3	0
Ce	139	161	143	9	201	0
Nd	56	69	56	10	78	1
Sm	11.3	14.7	11.5	8	16.1	2
Eu	2.1	2.5	2.6	4	3.6	0
Tb	1.40	1.50	1.63	3	2.45	1
Yb	6.2	7.2	6.1	10	8.6	3
Lu	0.97	1.19	0.95	9	1.35	3
Y	40	47	32	10	46	6

Figure 1

Click here to download Figure: Figure 1 .pptx

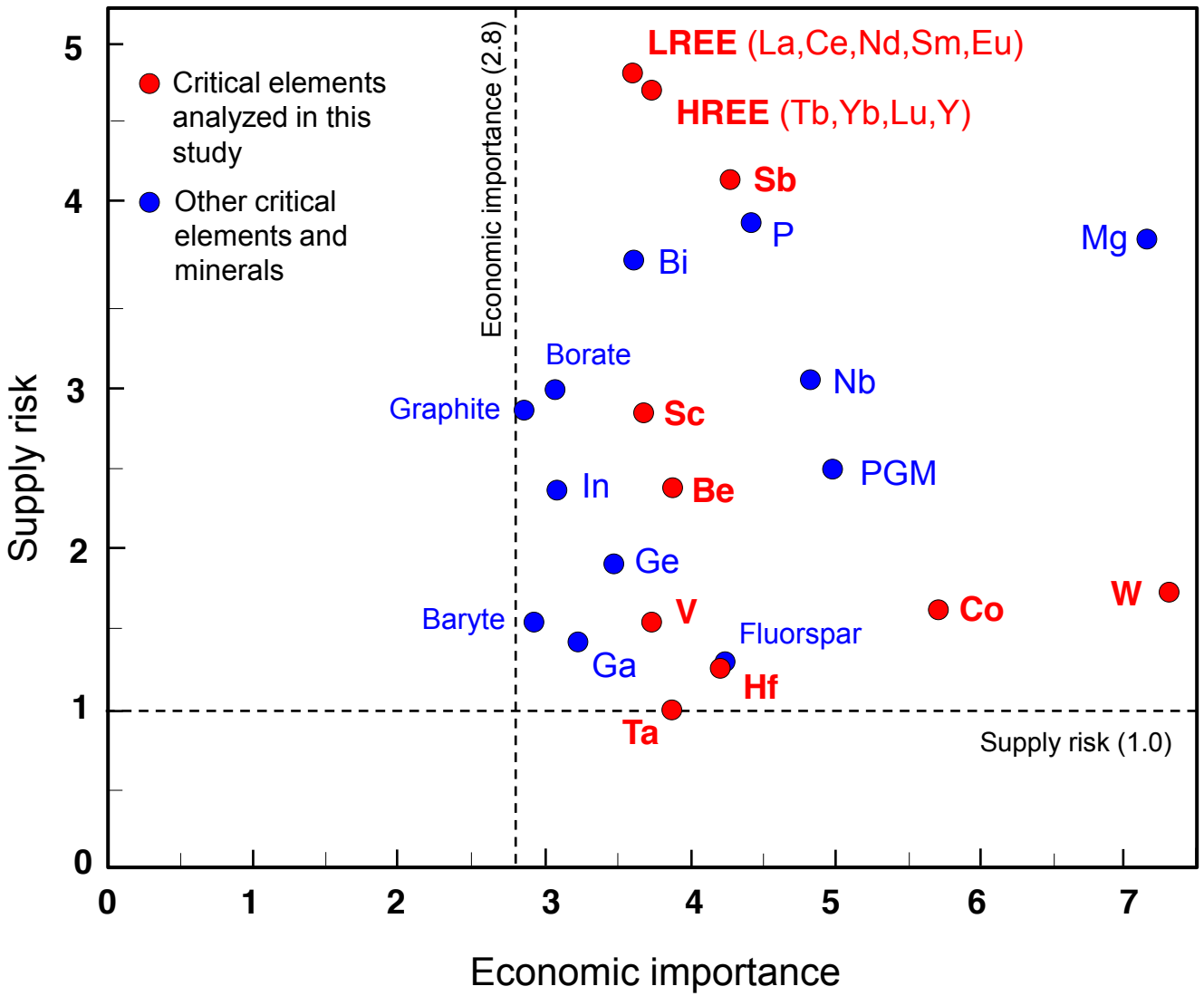

Figure 2

Click here to download Figure: Figure 2.pptx

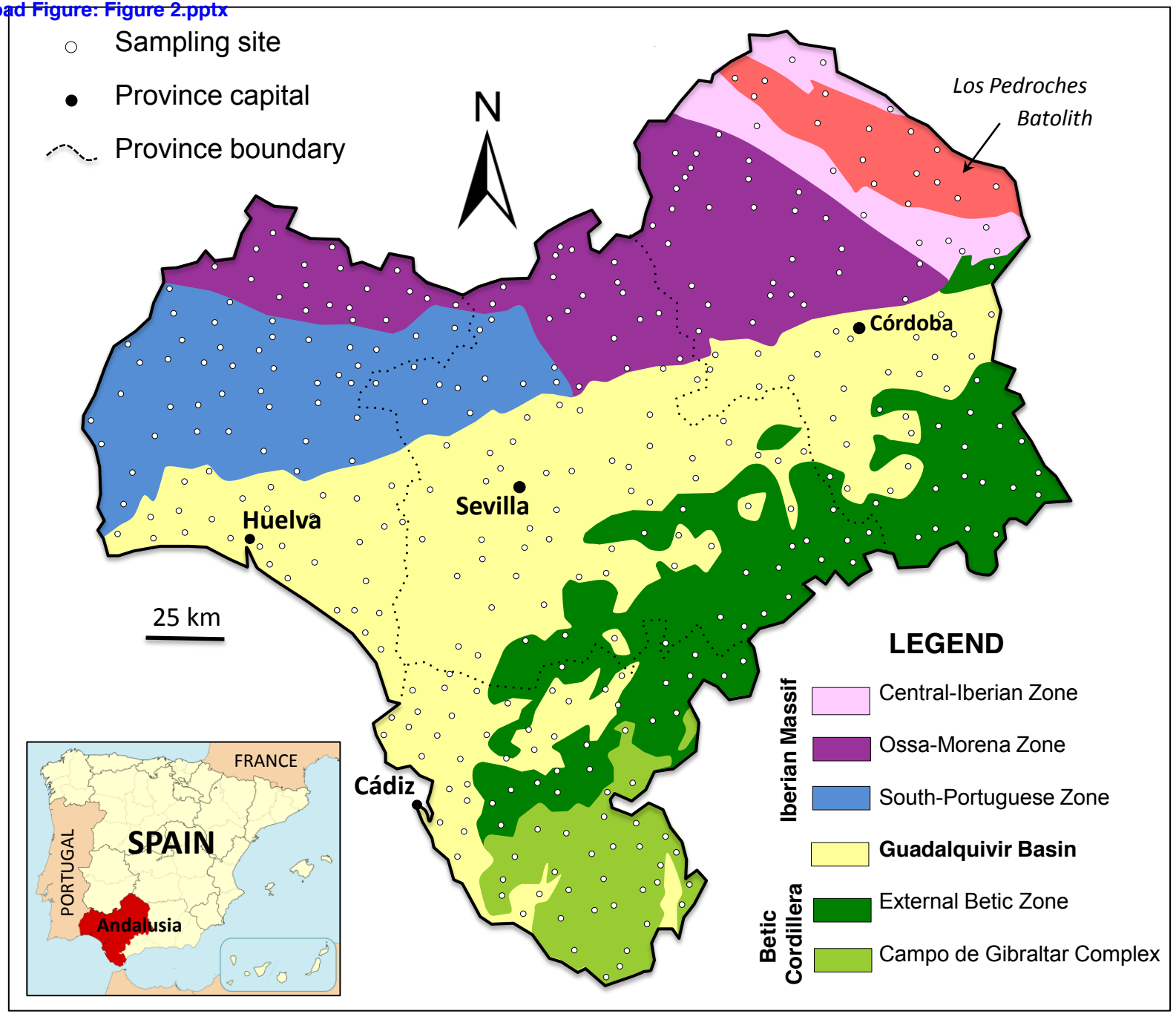

Figure 3

Click here to download Figure: Figure 3.pptx

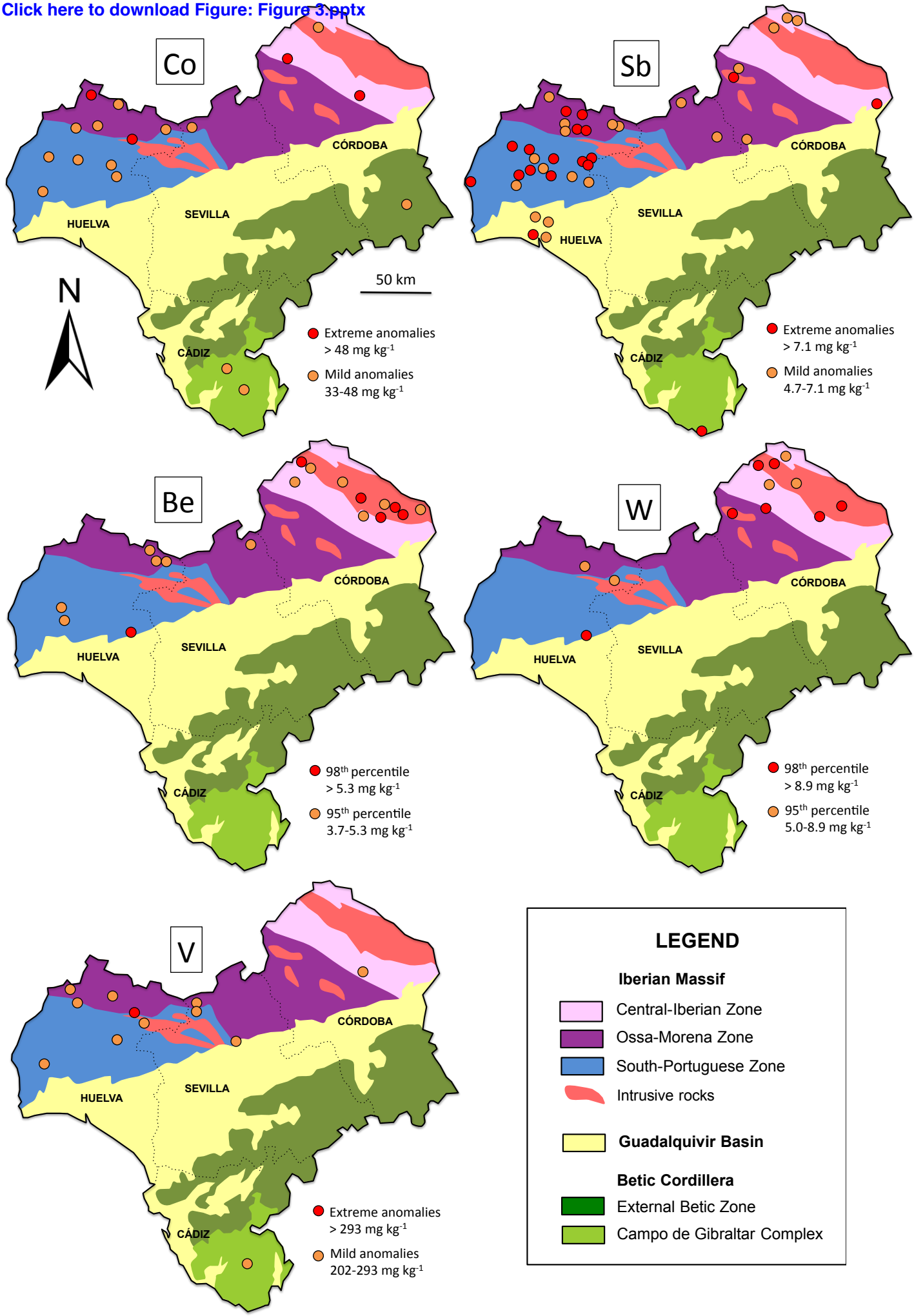

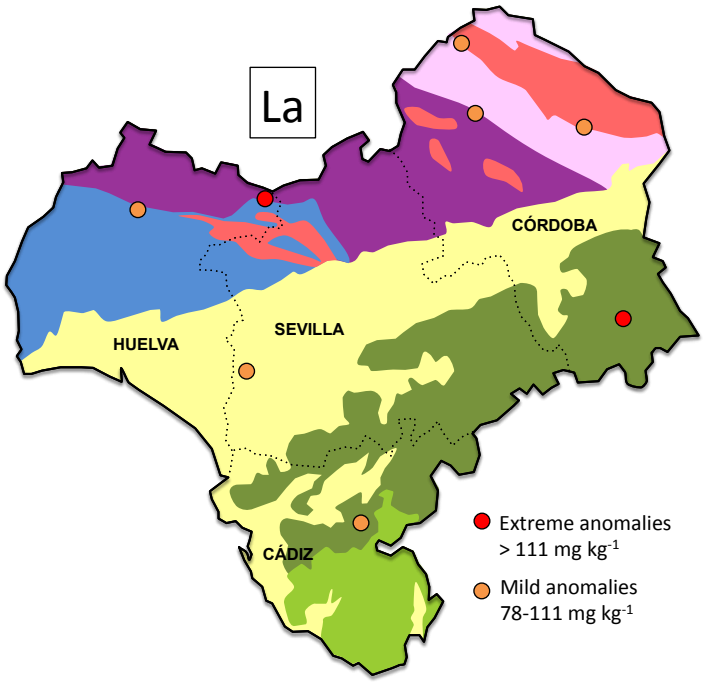
La
CÓRDOBA
SEVILLA
HUELVA
CÁDIZ
Extreme anomalies
> 111 mg kg-1
Mild anomalies
78-111 mg kg-1

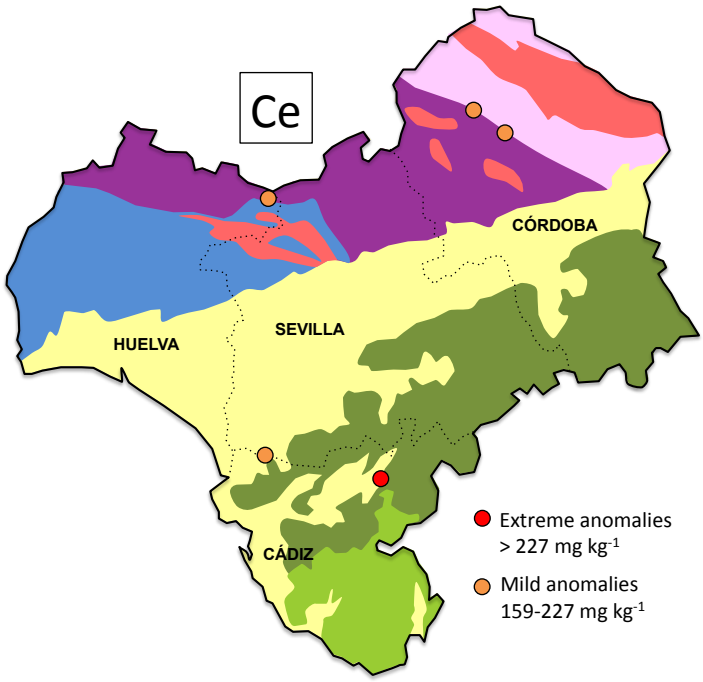
Ce
CÓRDOBA
SEVILLA
HUELVA
CÁDIZ
Extreme anomalies
> 227 mg kg-1
Mild anomalies
159-227 mg kg-1

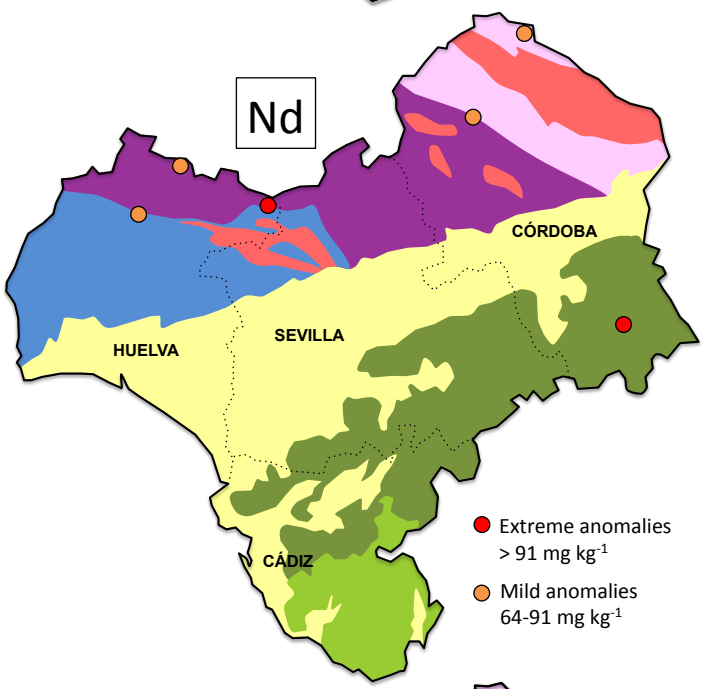
Nd
CÓRDOBA
SEVILLA
HUELVA
CÁDIZ
Extreme anomalies
> 91 mg kg-1
Mild anomalies
64-91 mg kg-1

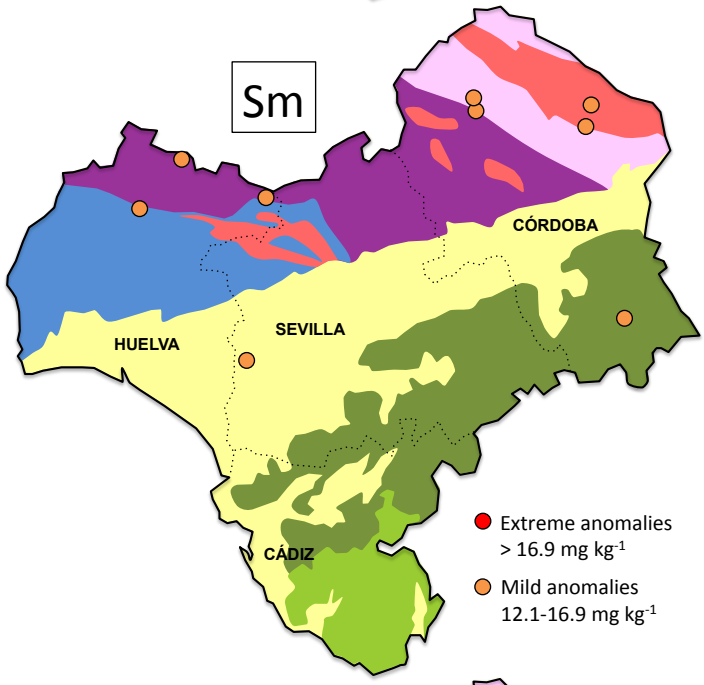
Sm
CÓRDOBA
SEVILLA
HUELVA
CÁDIZ
Extreme anomalies
> 16.9 mg kg-1
Mild anomalies
12.1-16.9 mg kg-1

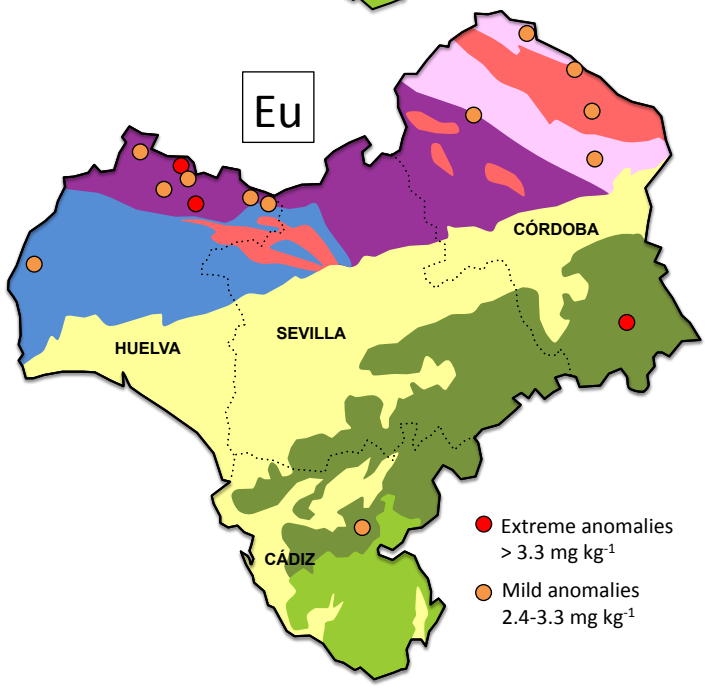
Eu
CÓRDOBA
SEVILLA
HUELVA
CÁDIZ
Extreme anomalies
> 3.3 mg kg-1
Mild anomalies
2.4-3.3 mg kg-1

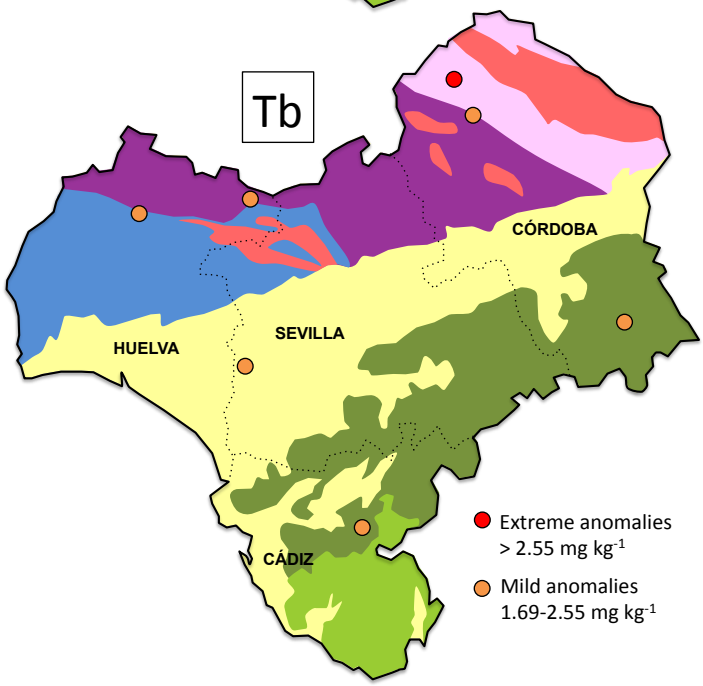
Tb
CÓRDOBA
SEVILLA
HUELVA
CÁDIZ
Extreme anomalies
> 2.55 mg kg-1
Mild anomalies
1.69-2.55 mg kg-1

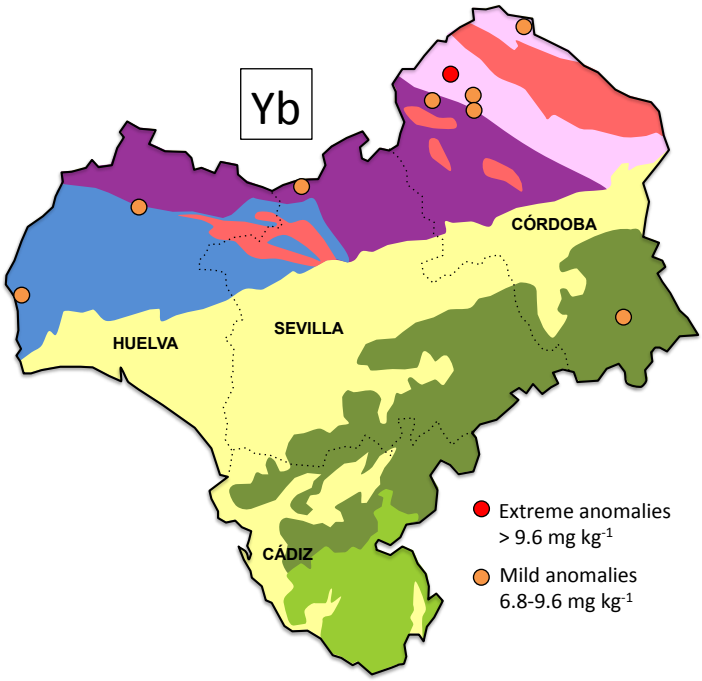
Yb
CÓRDOBA
SEVILLA
HUELVA
CÁDIZ
Extreme anomalies
> 9.6 mg kg-1
Mild anomalies
6.8-9.6 mg kg-1

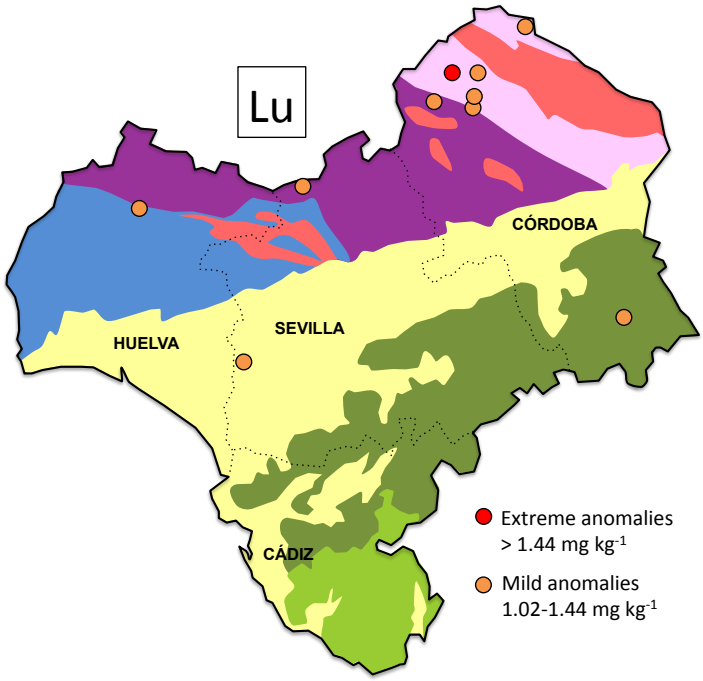
Lu
CÓRDOBA
SEVILLA
HUELVA
CÁDIZ
Extreme anomalies
> 1.44 mg kg-1
Mild anomalies
1.02-1.44 mg kg-1

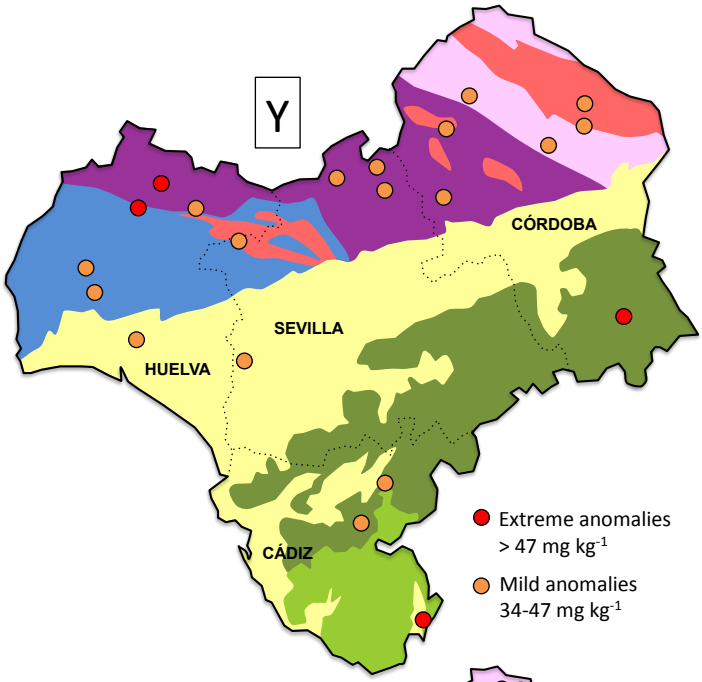
Y
CÓRDOBA
SEVILLA
HUELVA
CÁDIZ
Extreme anomalies
> 47 mg kg-1
Mild anomalies
34-47 mg kg-1

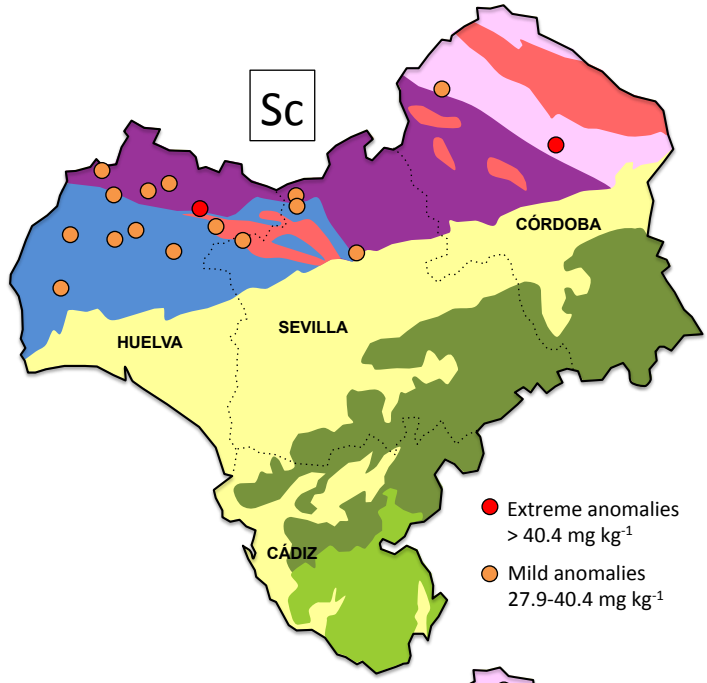
Sc
CÓRDOBA
SEVILLA
HUELVA
CÁDIZ
Extreme anomalies
> 40.4 mg kg-1
Mild anomalies
27.9-40.4 mg kg-1

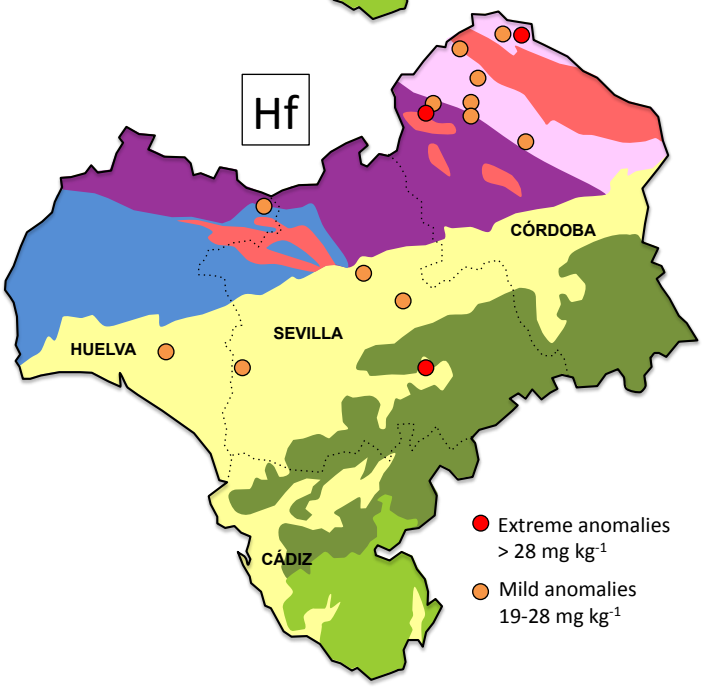
Hf
CÓRDOBA
SEVILLA
HUELVA
CÁDIZ
Extreme anomalies
> 28 mg kg-1
Mild anomalies
19-28 mg kg-1

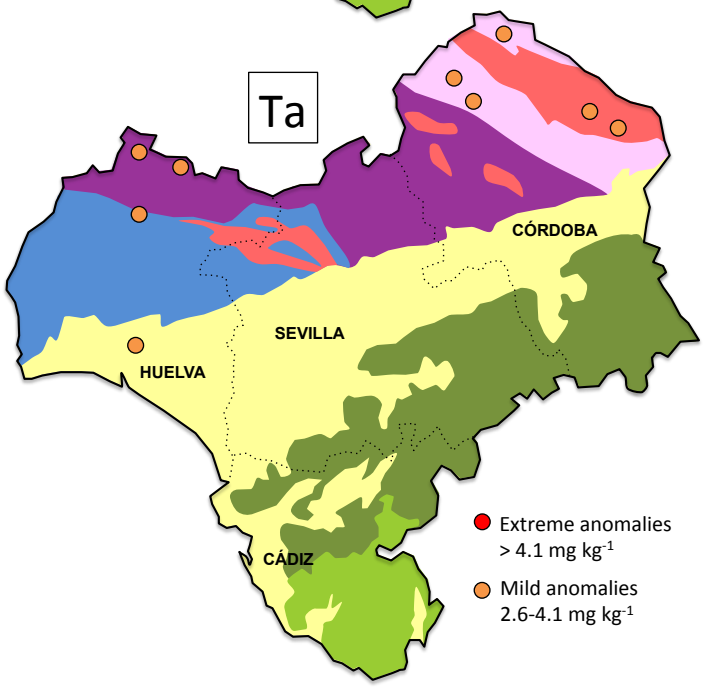
Ta
CÓRDOBA
SEVILLA
HUELVA
CÁDIZ
Extreme anomalies
> 4.1 mg kg-1
Mild anomalies
2.6-4.1 mg kg-1

Figure 4

Click here to download Figure: Figure 4.pptx

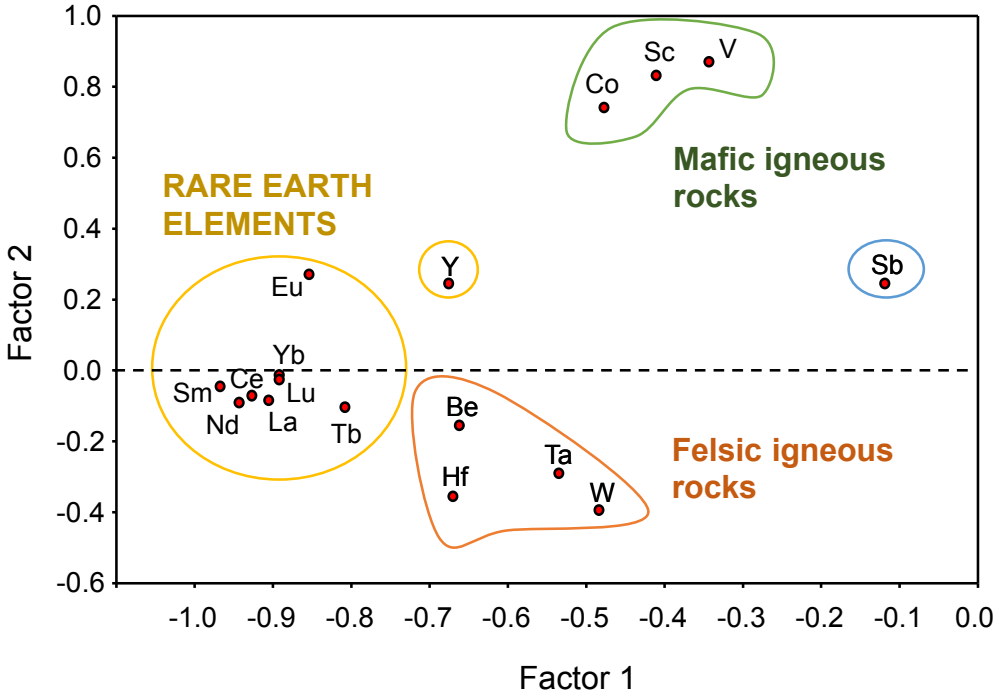

Figure 5

Click here to download Figure: Figure 5.pptx

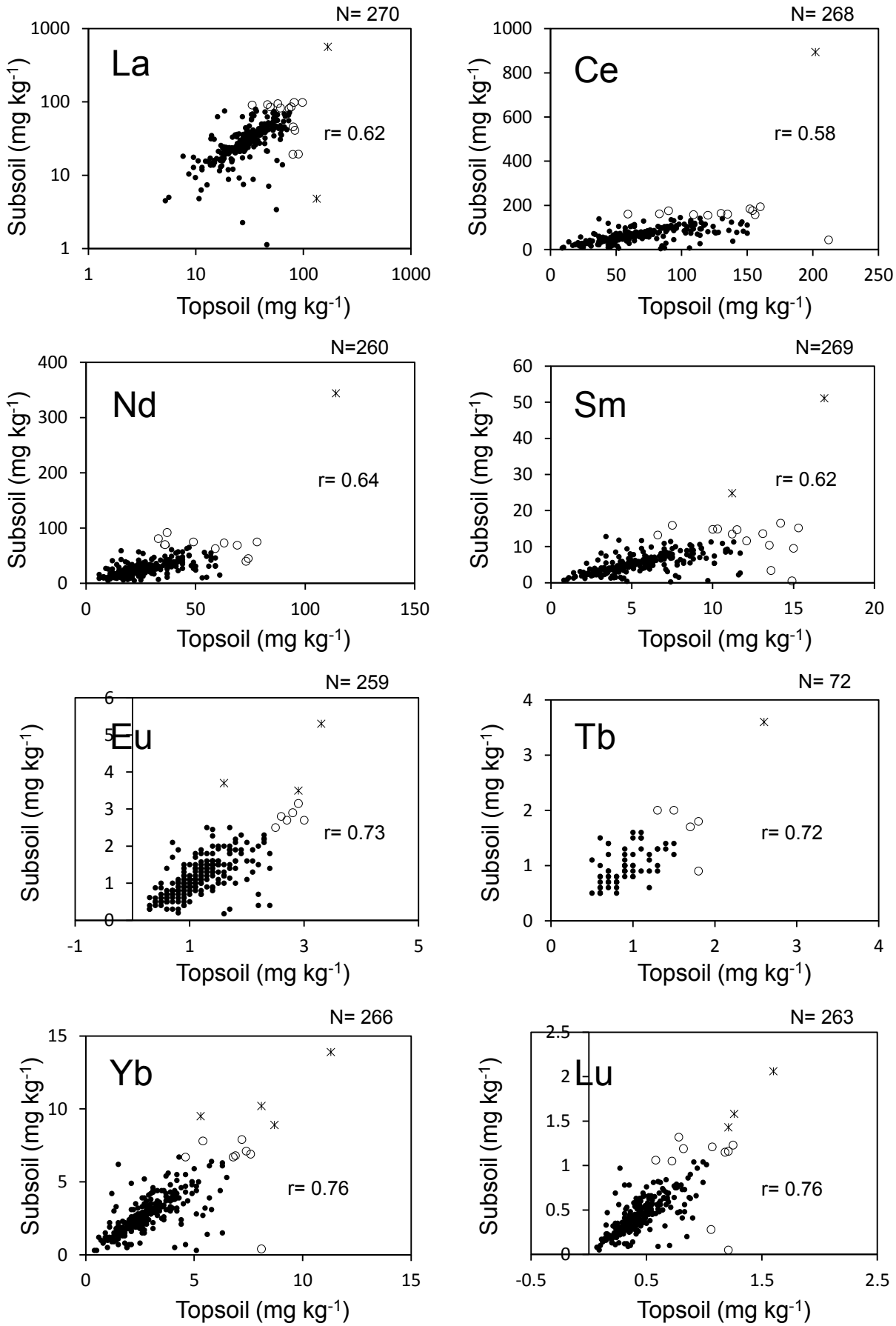

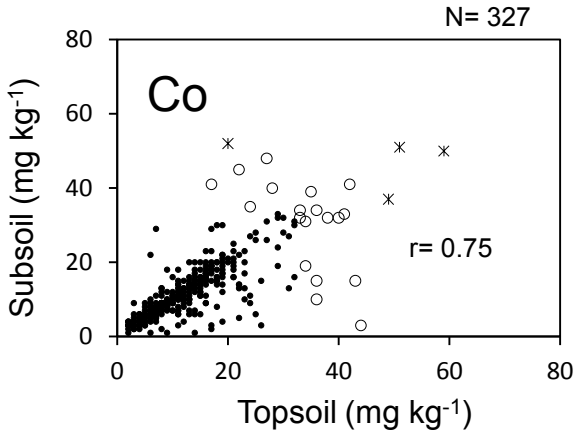
N= 327
Co
r= 0.75
Subsoil (mg kg-1)
Topsoil (mg kg-1)
0
20
40
60
80

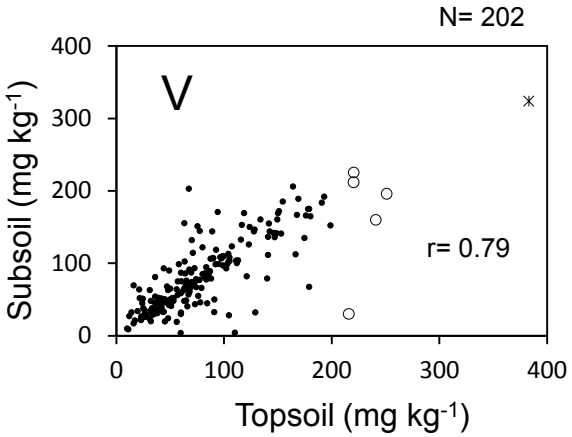
N= 202
V
r= 0.79
Subsoil (mg kg-1)
Topsoil (mg kg-1)
0
100
200
300
400

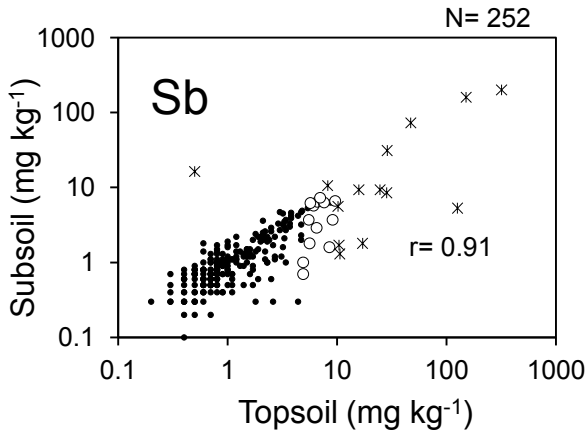
N= 252
Sb
r= 0.91
Subsoil (mg kg-1)
Topsoil (mg kg-1)
0.1
1
10
100
1000

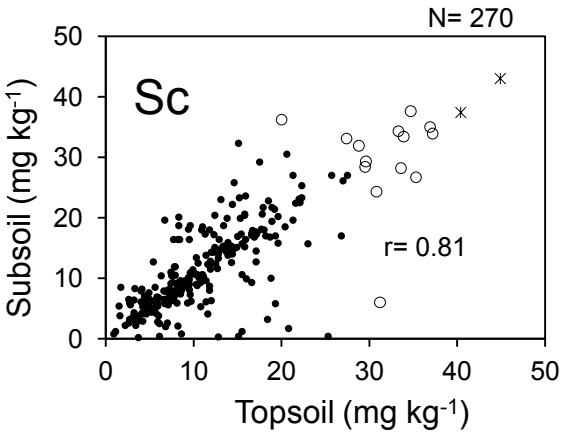
N= 270
Sc
r= 0.81
Subsoil (mg kg-1)
Topsoil (mg kg-1)
0
10
20
30
40
50

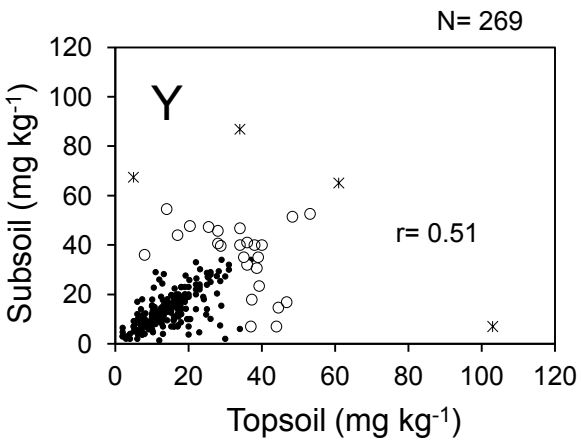
N= 269
Y
r= 0.51
Subsoil (mg kg-1)
Topsoil (mg kg-1)
0
20
40
60
80
100
120

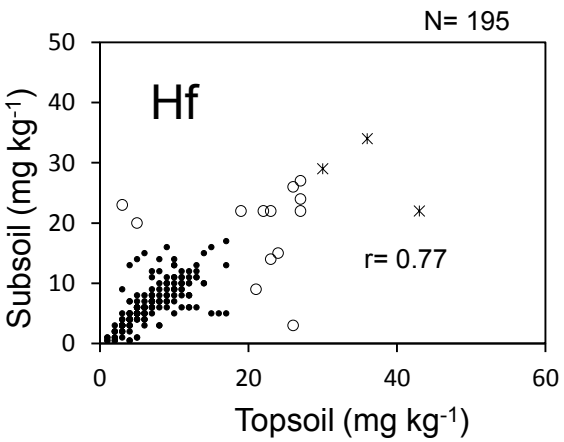
N= 195
Hf
r= 0.77
Subsoil (mg kg-1)
Topsoil (mg kg-1)
0
10
20
30
40
50
60

Figure 6

Click here to download Figure: Figure 6.pptx

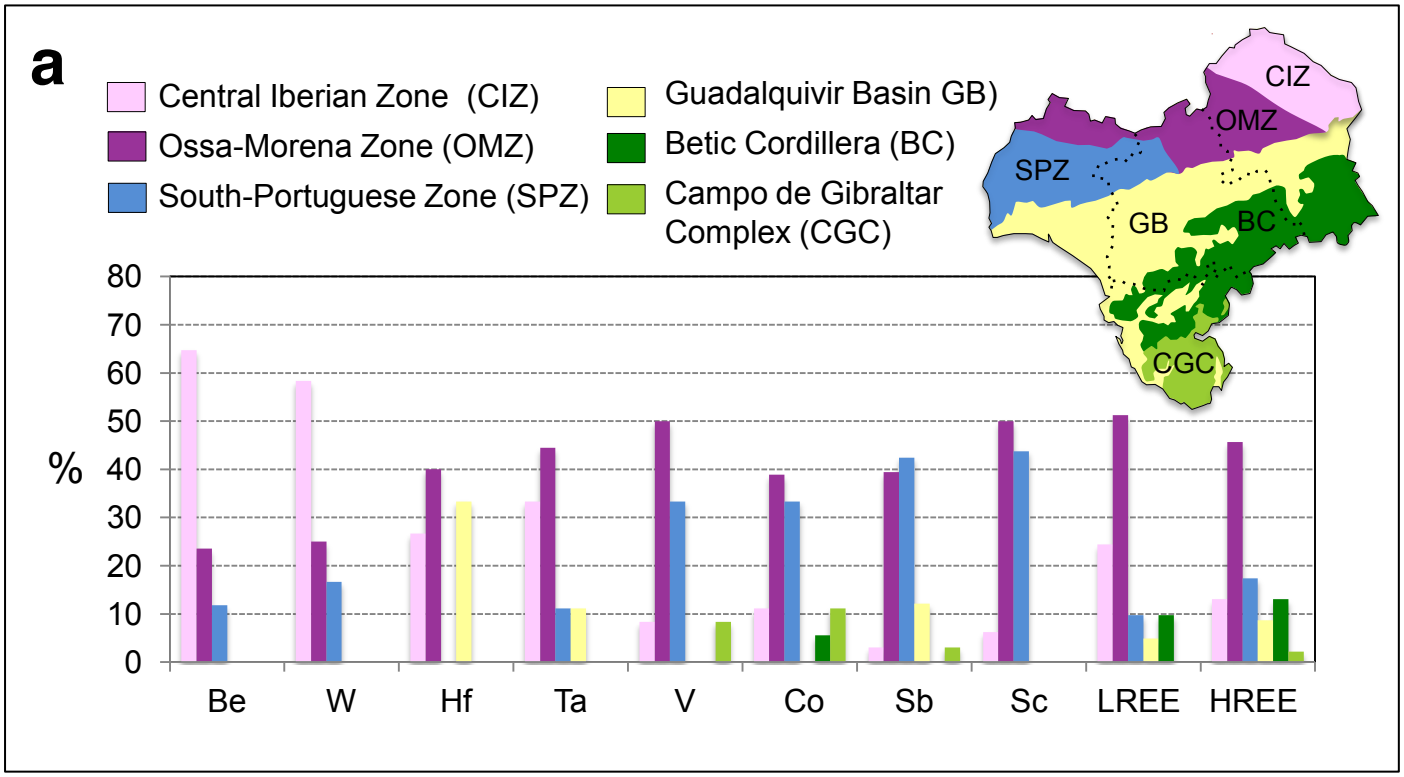

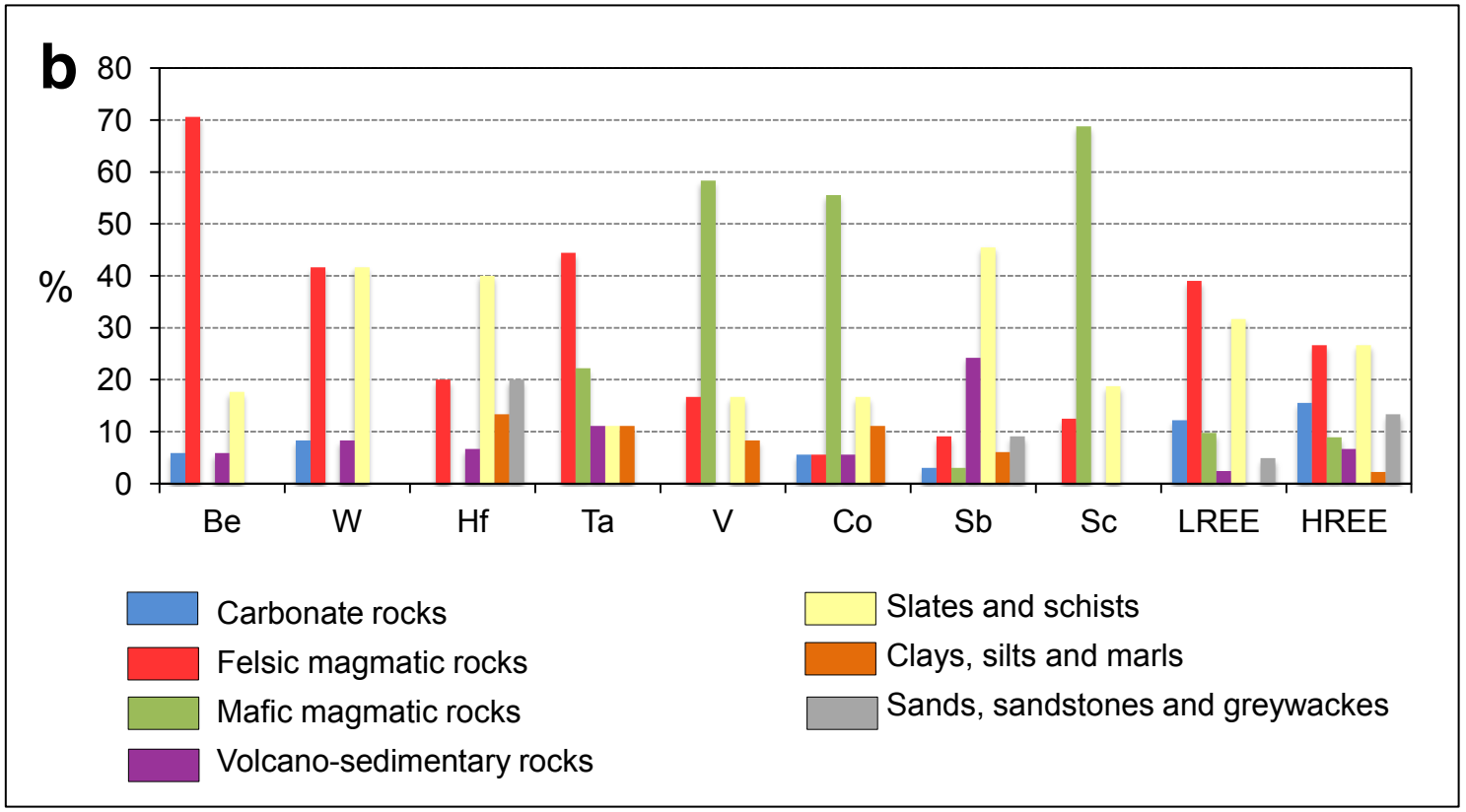
b
80
70
60
50
40
30
20
10
0
%
Be
W
Hf
Ta
V
Co
Sb
Sc
LREE
HREE
Carbonate rocks
Felsic magmatic rocks
Mafic magmatic rocks
Volcano-sedimentary rocks
Slates and schists
Clays, silts and marls
Sands, sandstones and greywackes

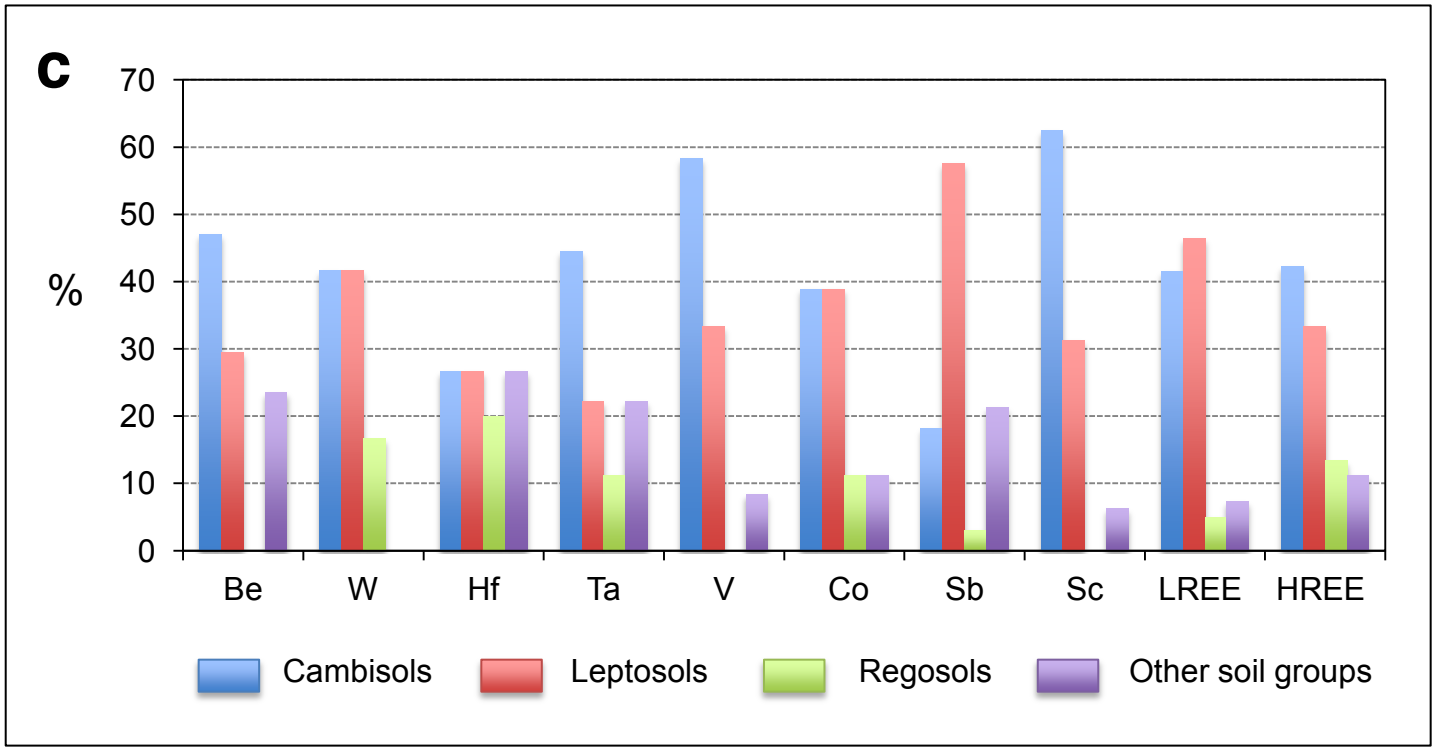
c
70
60
50
40
30
20
10
0
%
Be
W
Hf
Ta
V
Co
Sb
Sc
LREE
HREE
Cambisols
Leptosols
Regosols
Other soil groups

***Declaration of Interest Statement**

Declaration of interests

X The authors declare that they have no known competing financial interests or personal relationships that could have appeared to influence the work reported in this paper.

☐The authors declare the following financial interests/personal relationships which may be considered as potential competing interests:

CREDIT AUTHOR STATEMENT

J.C. Fernández-Caliani: Conceptualization, Methodology, Writing original draft preparation, Visualization, Formal analysis.

A. Romero: Visualization, Formal analysis, Reviewing and editing.

I. González: Methodology, Reviewing and editing.

E. Galán: Supervision, Project administration, Funding adquisicition.